Cardiovascular Magnetic Resonance and Multidetector Computed Tomography

13

Gabriel Vorobiof, Norman Elliot Lepor, Mark Doyle, Hee-Won Kim, and Gerald M. Pohost

Introduction

There have been considerable advances in cardiovascular cross-sectional imaging techniques. These include cardiovascular magnetic resonance (CMR) and multidetector computed tomography (MDCT) imaging. These technologies complement each other by allowing highly accurate and reproducible assessment of cardiac and vascular morphology and function.

Magnetic resonance (MR) provides the basis for and the newest of the imaging technologies. While magnetic resonance generates images with high resolution and high contrast without the need for contrast agent administration, most magnetic resonance systems available today must be gated to acquire high-quality images that demonstrate cardiac contraction. Newer systems, only recently available, allow acquisition of images at high speed, obviating the need for electrocardiographic synchronization. However, at present, gated studies offer superior resolution and image contrast, but either gated or "real-time" magnetic resonance images are optimally suited to visualize the heart and its contractile function. Magnetic resonance angiography (MRA) is excellent for rapidly evaluating the aorta and the peripheral arteries and can be acquired and displayed in 2-D and 3-D. MRI can precisely characterize cardiac function and quantify ventricular volumes, right and left ventricular ejection fraction, and left ventricular mass and can quantify pressure gradients across stenotic valves, regurgitant fractions, and shunt fractions in patients with intracardiac shunts. Valve morphology and area can also be evaluated and the severity of valvular stenosis quantified. Cardiac MR is also useful for identifying cardiac masses, pericardial abnormities, and congenital heart disease. In certain disease states, such as myocardial infarction and cardiomyopathies, the resolution of MRI is further improved by the addition of extrinsic contrast agents. Cardiac MRI is also very useful in assessing paramagnetic contrast agents that cause a reduction in the T1 relaxation time leading to increased signal intensity on T1-weighted images and are typically small molecular weight compounds containing as their active elements gadolinium, manganese, or iron. All of these elements have unpaired electron spins in their outer shells and long relaxivities. Magnetic resonance spectroscopy (MRS) allows assessment of the metabolic responses of the myocardium most commonly by using the proton (H-1) and the phosphorus-31 (P-31) spectra. Phosphorus-31 spectroscopy can assess the conversion of energy through oxidative phosphorylation during myocardial work by evaluating high-energy phosphate. Proton MRS of the heart, despite high sensitivity of the proton metabolites, has not been readily applicable for clinical utility due to technical challenges including signal suppression of the huge water resonance peak and identification of the methyl and methylene group of the lipid.

G. Vorobiof, MD, FACC
Division of Cardiology, Department of Medicine,
David Geffen School of Medicine at UCLA,
Los Angeles, CA, USA

N.E. Lepor, MD
Cedars-Sinai Heart Institute,
Beverly Hills, CA, USA

M. Doyle, PhD
Department of Medicine, Allegheny General Hospital,
Pittsburgh, PA, USA

H.-W. Kim, PhD
Department of Radiology,
University of Southern California,
Los Angeles, CA, USA

G.M. Pohost, MD, FAHA, FACC (✉)
Department of Radiology,
Keck School of Medicine, University of Southern California,
Beverly Hills, CA, USA

Department of Medicine,
School of Medicine, Loma Linda University,
99 N. LaCienega Boulevard,
Beverly Hills 90211, CA, USA
e-mail: gerry2710@yahoo.com

C. Rosendorff (ed.), *Essential Cardiology*,
DOI 10.1007/978-1-4614-6705-2_13,

Magnetic Resonance Imaging

Principle of Nuclear Magnetic Resonance

When an atomic nucleus contains an odd number of subatomic particles (i.e., protons plus neutrons), it possesses a property known as "spin." The nucleus can be imagined to spin around its axis in a manner similar to the rotation of the earth. When electrical charges (in this case, the atomic nucleus) move, a magnetic field is generated. Intrinsic magnetic fields of atomic nuclei can interact with externally applied magnetic fields. Sensitive atomic nuclei placed within an extrinsic magnetic field will align either *with* or *against* that field. Quantum mechanical considerations dictate that for any macroscopic amount of material, slightly more nuclei will align with the field than will be antialigned. Thus, material placed in an external magnetic field will attain a bulk magnetic field strength. Stronger fields generate higher numbers of nuclei that preferentially align. If the nucleus is disturbed—for example, by applying a radio frequency (RF) field—it will displace from alignment with the extrinsic magnetic field. When the RF energy is terminated, the disturbed nuclei continue to precess. *Precession* is the relatively slow "wobbling" phenomenon that is observed with a child's spinning top or a gyroscope. In a similar manner, nuclei with intrinsic "spin" and a magnetic moment will precess in an external magnetic field. The frequency of precession depends on the strength of the magnetic field (B_0) and the nuclear characteristics (gyromagnetic ratio, γ) of a given element. The RF field has to be applied at the precession frequency (i.e., at the resonance frequency for the system, which is also known as the Larmor frequency). The phenomenon of nuclear MR (NMR) is manifested when a substance with magnetically sensitive nuclei (e.g., the nucleus of hydrogen-1 [proton], phosphorus-31, fluorine-19, or sodium-23) that is placed in a strong magnetic field is momentarily pulsed with RF energy at the resonance frequency. The nuclei of all these atoms are naturally abundant and stable (i.e., not radioactive). While virtually all MR images are derived from the hydrogen nucleus (ubiquitous in water), researchers have created cardiac images of less-abundant signal sources, such as the natural sodium-23 distribution. During the process of free precession (i.e., after termination of the RF field), nuclei give off a detectable signal. This RF signal is detected by a conducting coil placed close to the sample [1].

The units of magnetic field strength are the gauss (G) and the tesla (T). The strength of the earth's magnetic field is on the order of 0.5 G. A typical commercial MR system useful for cardiovascular studies has a field strength of 15,000–30,000 G. It is customary to express field strength with NMR in tesla units (1 T = 10,000 G). Thus, 15,000 G is equivalent to 1.5 T.

Importance of Radio Waves or Radio Frequency

RF pulses are delivered at the resonant or Larmor frequency:

$$\omega = \gamma B_0$$

For protons, γ= 42.58 MHz/T. Typical spin-echo pulses reorient the net magnetism of the nuclear spins by 90 or 180°. Faster and newer imaging techniques used for cardiovascular MR apply pulses of short duration, with net spin reorientation of less than 90°. Following the RF pulse, the net magnetization precesses at the Larmor frequency. As individual spins precess, they emit an RF signal, which is detected by an RF coil. The frequency of these radio waves is characteristic for a given atomic nucleus and is affected by the chemical milieu. The detected radio waves are digitized and converted into signal peaks, or spectra, by application of the mathematical process known as *Fourier transformation*. The chemical milieu can cause the location of a resonance peak in the spectra to appear at a slightly different position than indicated by the field strength, B_0, a phenomenon known as chemical shift. Thus, the three phosphorus peaks of adenosine triphosphate (ATP) are located in different spectral frequencies on phosphorus-31 spectrum, and the hydrogen peak of water and of fat are in different spectral frequencies in the proton spectrum.

The intrinsic magnetic field produced by the tissue will gradually reorient and realign with the extrinsic field after perturbation by the RF pulse and is said to *relax*. There are two relaxation times: T1 (or spin–lattice relaxation), which is related to the time required for the net magnetization of the sample to realign with the main magnetic field by 63 % (i.e., $1 - 1/e$), and T2 (or spin-spin relaxation time), which is related to the time required for spins that were originally in phase with the applied RF pulse to lose phase coherence by 63 % (i.e., $1 - 1/e$). The concentration of the nuclei (spin density) and the relaxation times T1 and T2 determine the magnitude of a peak in the spectrum or the intensity of a pixel in an image. Other variables that affect signal intensity are motion, flow, chemical shift, and magnetic susceptibility. Previously, image contrast was derived from a "weighting" toward one of these parameters, for example, a T1-weighted image was obtained using a high RF flip angle and a rapid repetition such that only spins with very short T1 relaxation substantially contributed to the image signal. There is a growing trend to obtain images in which these spin characteristics are quantitatively represented. Typically this involves "mapping" out the exponential character of the T1 or T2 relaxation curves. When applied to cardiac tissue, due to the heart motion, these techniques tend to be either time-consuming or of limiter accuracy. However, the importance of quantitative parameter imaging is likely to increase as time goes on.

Whereas spectroscopy utilizes differences in chemical shift of each metabolite in a uniform magnetic field, imaging

utilizes externally applied magnetic field gradients. The key to imaging is to vary the magnetic field strength as a function of spatial location. This is accomplished by applying a linear magnetic gradient along each axis in which spatial differentiation is required. Each gradient either adds to or subtracts from the main magnetic field, producing a continuous variation in resonance frequency along the sample. Application of the Fourier transform to signals acquired in the presence of linear gradients directly translates this range of frequency information into spatial intensity data and forms the basis of imaging and angiography. Control of the gradients allows slice selection to be achieved in any orientation.

Instrumentation for Magnetic Resonance Studies

A CMR system consists of a large (typically cylindrical) superconducting magnet, an RF coil that fits within the bore of the magnet; RF receiver coils, gradient coils that generate the magnetic fields needed to create images; and an image-processing computer (Fig. 13.1). The large magnet contains multiple coils of niobium titanium, which has essentially no resistance to electrical current when it is supercooled. Such supercooling takes place when the coils in the magnet are bathed in liquid helium at 4 °K or −269 °C. While permanent, "open" magnets are also available for CMR, high-field superconducting magnets are preferable for the resolution and speed required for cardiac applications. The imaging gradient coils are located within the magnet bore and are used to vary the magnetic field in a precisely controlled manner. They introduce controlled variations in magnetic field related to the position of an organ or a portion of an organ within the magnet. Having the ability to rapidly switch the gradient coils on and off allows rapid acquisition of cardiovascular images. The cylindrical body RF coil also fits concentrically within the bore of a cylindrical magnet and transmits the radio waves needed to create a spectrum or an image. A smaller multielement coil placed over the heart or vascular bed of interest is used to receive the RF signal with high sensitivity (the combination of receiver element and sampling hardware is referred to as a "channel"). There are so-called parallel imaging techniques that utilize the independence of the multiple channels to speed up the image acquisition at the expense of losing signal to noise. Naturally, coordination of this complex system requires extensive computer control of the gradient and RF amplifiers and the vast array of associated electronic components. Typically, an operator's console is placed in a room adjacent to the scan room, allowing visual contact with the patient environment via a window. The console provides a convenient means to alter the acquisition methods, RF pulse sequence, and view selection.

A spin-echo image of the heart typically is acquired with high spatial resolution in which moving blood appears as a signal void or as a "dark-blood" region. A gradient-echo pulse sequence typically generates images at higher speed and with "bright blood." The dark-blood approach is ideal for assessing cardiac morphology, whereas the bright-blood approach is appropriate for assessing ventricular function. When turbulence occurs in the bloodstream, bright-blood images demonstrate a localized reduction in brightness directly associated with the turbulence. For example, the jet associated with mitral or aortic regurgitation is visualized as a dark region against otherwise bright blood, owing to signal dephasing. Newer systems have higher-speed imaging capabilities such as "echo planar" and spiral imaging, which are capable of generating an image in under 30 ms, but presently, these images are of generally low resolution. Both dark-blood and bright-blood imaging can be performed with cardiac gating to freeze heart motion at certain phases in the cardiac cycle, thus allowing higher-resolution images to be acquired, but at the expense of increased scan time. Typically, in cardiac gated sequences, 20–30 frames representing the cardiac cycle are acquired. In general, cardiac cine sequences are based on bright-blood gradient recalled echo (GRE) approaches, or a variant termed steady-state-free precession (SSFP). In this way both regional and global ventricular performance can be evaluated. A typical GRE sequence requires 10–15 s acquisition time and can be acquired within a breath hold. Using GRE methods, a series of images can be acquired throughout the cardiac cycle and then assembled in sequence in the computer as a cine loop that can be replayed repeatedly to allow evaluation of wall motion (Fig. 13.2).

Since its introduction into routine clinical practice, steady-state-free precession (SSFP) imaging has evolved in a number of different forms that efficiently combine the gradient and spin-echo components to increase blood signal contrast. These approaches, variously and imaginatively termed FIESTA, true FISP, balanced FFE, and others, have resulted in excellent blood-myocardial contrast, almost independently of blood flow characteristics. Both dark-blood and bright-blood imaging sequences are performed in conjunction with cardiac gating to effectively freeze the motion of the heart at distinct phases within the cardiac cycle.

Older CMR systems have rather long cylindrical magnets. Some patients (as many as 5 %) are unable to tolerate such an enclosure due to claustrophobia. Anxious patients can be given a mild sedative such as benzodiazepine. Most modem systems have shorter magnet length and a wider bore and are thus more "patient friendly." Again, even on newer systems the gradients can be quite noisy. This is especially true for the fast imaging sequences used in cardiovascular MR. Earplugs are always required to protect the patient from noise-related hearing damage. Newer systems incorporate substantial sound dampening to isolate the gradient vibrations from the system, thus reducing noise to some extent. An intercom system is used to maintain verbal contact

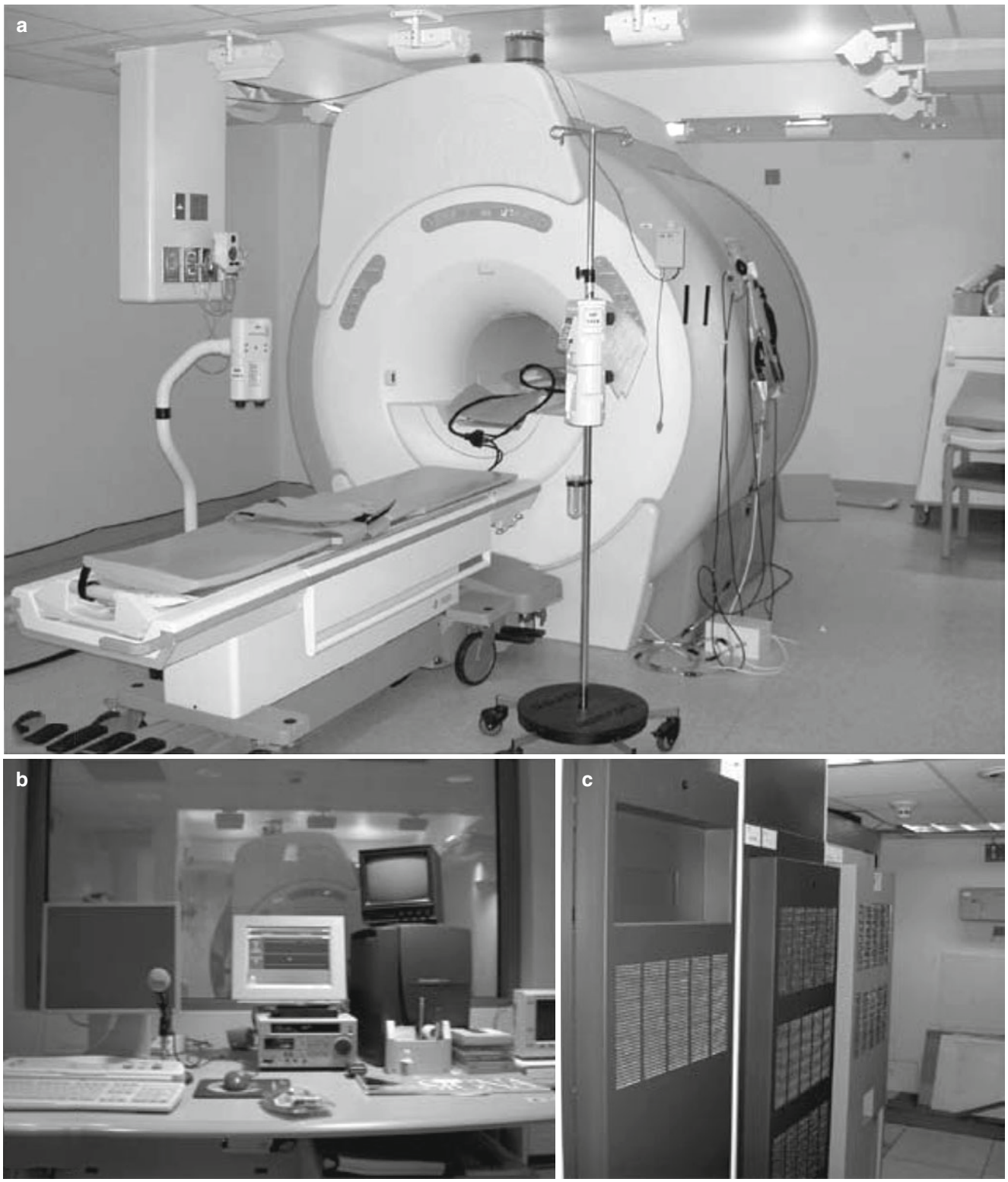

Fig. 13.1 Composite photograph of major components of a typical MRI system. (**a**) Scanner magnet and patient table; the table accommodates patient entry, exit, and positioning within the magnet bore. (**b**) Operator's console, which is remote from the scanner, allows control of scanner functions and incorporates an image and physiologic data viewing station. (**c**) Bulky hardware to power the scanner is typically located in a separate room; components include gradient and RF power units and the controlling computer

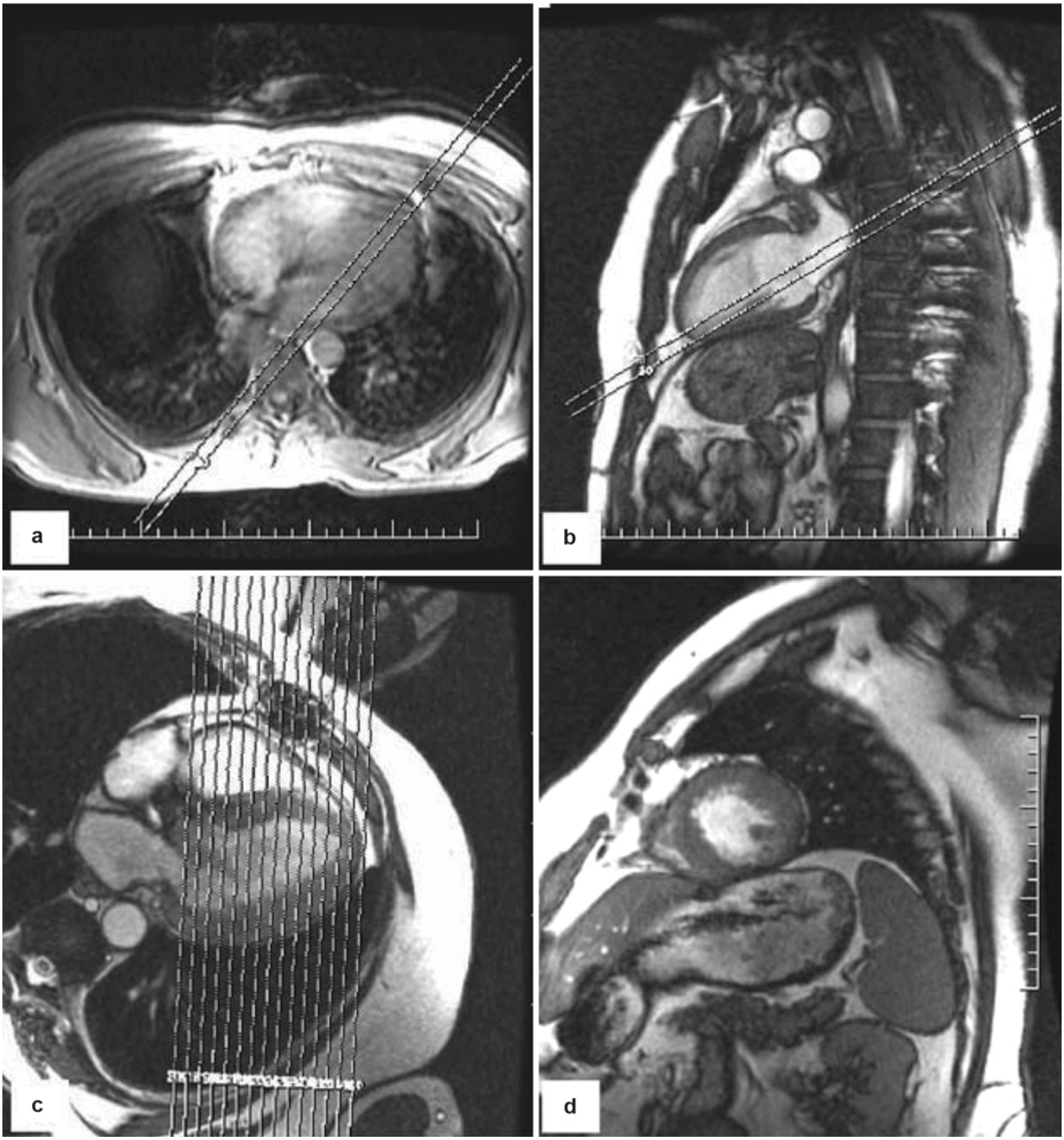

Fig. 13.2 Sequence of scans required to obtain standard cardiac views. (**a**) A noncardiac-triggered spin-echo transverse scout is obtained and is used to plan the two-chamber view. (**b**) The two-chamber view of the left ventricle is in turn used to plan the four-chamber view. (**c**) The four-chamber view is in turn used to plan the multiple-slice short-axis views. (**d**) A short-axis view of the left and right ventricles. Views (**b** and **d**) were obtained in cine mode using steady-state free precession imaging

between system operator and patient. This is important, to inform the patient of important events during the examination such as table movements, injections of contrast agents, or stress agents. Verbal communication is especially important to direct the patient with the appropriate timing for breath holding during image acquisition. Special MR-compatible (e.g., nonmagnetic) systems are required for physiological monitoring of the patient during an examination. This is especially important if the patient receives pharmacological stress while within the bore of the magnet.

While a uniform body coil is required to optimally transmit RF energy into the body, the most important characteristic for signal reception is maximization of the signal-to-noise ratio. This can be accomplished by positioning a receiver coil system on the body's surface. A typical reception system consists of a number of separate coils that are essentially positioned or wrapped around the thorax (for cardiac imaging). This composite coil is made up of a number of smaller sub coils, each requiring its own signal reception electronics, and is referred to as a phased array system (the number of coil elements relating directly to the number of channels). Importantly, recent advances have allowed reduction in scan time by separately processing the signal from each coil in parallel, to essentially construct a separate part of each full image. These parallel imaging approaches cause a slight reduction in signal-to-noise ratio, but typically can reduce the scan time by factors of 2 or 4. These approaches are generically known under various trade names including ASSET, SMASH, and SENSE.

In addition to the inherent contrast produced by each imaging sequence, it is possible to augment contrast by means of "spin preparation pulses." Preparation pulses are typically applied to produce contrast dependent on the T1 relaxation process. At 1.5 T the T1 value of myocardium (water signal) is approximately 850 ms, while that of fat tissue is about 300 ms. Application of an RF pulse to invert the spin system will initially invert both the water and fat signals. However, as the spin system relaxes to its equilibrium condition, the fat signal relaxes faster than the water signal. By carefully selecting the time following the inversion pulse at which to perform the imaging sequence, it is possible to "null" either the fat or the water signal. The process of inverting the signal and waiting for it to partially recover before performing imaging is referred to as "inversion recovery" (IR).

Currently, there is some debate concerning the utility of higher-field imaging systems (e.g., 3 T systems) for cardiac imaging purposes. The potential advantage is that the SNR is higher, but the downside is that RF energy is higher (leading to heating) and sources of artifact are higher (related to the susceptibility/inhomogeneity introduced by the high magnetic field). At the time of writing, there is no clear indication for cardiac imaging and higher fields.

Further, it is possible to alter the T1 of tissue by administration of a contrast agent. These nonionic agents typically contain a gadolinium chelate, which, when it comes in close contact with tissue, effectively reduces the tissue's T1 by introducing a highly localized, randomly varying, magnetic field gradient. Contrast agents have application areas varying from allowing visualization of myocardial perfusion, imaging the vasculature, differentiating between masses, and identifying viable and nonviable myocardium with high accuracy.

Current Applications

CMR and MRA are excellent for assessing both cardiac morphology and function. CMR has the unique ability to acquire images of the heart in any tomographic plane that is preselected by the operator at the console. However, it is customary to acquire imaging planes through the vertical long axis (two-chamber view), the horizontal long axis (four-chamber view), and the short axis (Fig. 13.2). At the present time, magnetic resonance imaging and angiography are excellent for assessing global and regional left and right ventricular size and performance; for evaluating the abnormal morphology and physiology found in congenital heart disease, including intra- or extracardiac shunt quantification; for characterizing myocardial tissue, such as in arrhythmogenic right ventricular cardiomyopathy; for assessing myocardial wall thickness and ventricular volumes and geometries in the cardiomyopathies and in valvular heart disease, particularly to interrogate velocities; for the assessment of the pericardium, particularly differentiation of constrictive pericarditis from restrictive myocardial disease; for cardiac/paracardiac masses; for comprehensive evaluation of aortic dissection and aortic aneurysms; and for assessment of the larger arterial branches from the aorta such as the carotids, the renals, the iliofemorals, and more recently, the coronary arteries with and without contrast. CMR has been demonstrated to be clinically effective in myocardial perfusion and is considered to be the gold standard for myocardial viability.

Cardiac chamber size, myocardial wall thickness, and mass are readily assessed from CMR images. Chamber morphology, orientation, and relationships to the great vessels and viscera are easily assessed. In addition, atrioventricular, venoatrial, and ventriculoarterial connections can readily be defined and evaluated in terms of anatomy and hemodynamics. Three-dimensional contrast-enhanced cardiac views can be rotated and viewed from any orientation. Such capability is ideal for assessing complex congenital heart disease.

Many of the current applications of EBCT and MDCT are similar to those described for CMR but also include assessment of the presence, extent, and location of calcified and noncalcified coronary artery plaque.

- Global and regional left and right ventricular function
- Assessing myocardial wall thickness and ventricular volumes and cardiomyopathies
- Assessment of coronary artery anatomy and stenosis
- Assessment of coronary calcium to detect atherosclerosis
- Assessment of myocardial ischemia and infarction
- Assessment of aorta and the larger arterial branches
- Comprehensive evaluation of aortic dissection and aortic aneurysms
- Evaluating congenital heart disease, anatomy, and conduit patency
- Assessing cardiac and paracardiac masses
- Assessing the pericardium and pericardial effusion or constriction

Table 13.1 CMR EBCT and MDCT: respective clinical applications

	MRI	EBCT and MDCT
Cardiac morphology	Excellent intrinsic soft tissue and blood contrast allows delineation of anatomic features with good resolution. No external contrast required	Requires administration of contrast agent to delineate blood pool features, but provides good anatomic depiction
Ventricular (and other chamber) function	Excellent temporal and spatial resolution with any orientation allows optimal evaluation of contractile function; RF tags provide further delineation of regional wall function	Requires contrast agent to distinguish blood pool, limited angulation available, but 3-D images can be generated with good resolution
Coronary anatomy	Breath-hold techniques allow coronary artery location to be traced to origin	Contrast techniques allow coronary artery trajectory to be traced to origin
Myocardial perfusion	Myocardial perfusion, in later stages of development	Myocardial perfusion by tracking a bolus of radiopaque contrast
Pericardial disease	Allows differentiation between restrictive and constrictive disease (i.e., generally, myocardial vs. pericardial). MR is a "gold standard" for assessing pericardial thickness. Able to determine physiologic significance, even in absence of thickened pericardium	MDCT is able to distinguish between myocardium and pericardium similar to CMR
Valvular assessment	Can assess valve function, visualize turbulent flow, and approximate the severity of regurgitation and stenosis	Unable to visualize turbulence, must rely on ancillary data (quantifying differences in stroke volumes between LV and RV)
Metallic artifacts	Signal void	Streak artifacts
Cardiac masses	Can be easily detected as filling deficits within the cardiac blood pool, important role for T1 and T2 tissue characterization	Can be identified after a contrast bolus
Contrast agent	Chelates of gadolinium and dysprosium with no known adverse effects	Iodinated contrast—many adverse side effects: renal failure, anaphylaxis, or pulmonary edema
Angiography of the arterial system:	No need for contrast agent although early data suggests contrast markedly shortens acquisition time and further increases resolution	Radiopaque iodinated contrast agent required
Aorta	++++	+++
Aortic arch	++++	+++
Carotid and cerebral arteries	++++	++
Peripheral arteries and veins	++++	+++
Coronary calcification	Not well visualized; calcium has little CMR signal due to its solid state	Easily visualized without contrast administration
High-energy phosphate metabolism	Yes	No
	No	Yes

Table 13.1 contrasts/compares these technologies in their respective applications.

Ventricular Function Chamber Size and Wall Thickness

CMR Techniques

Global and regional right and left ventricular function can be assessed using cine GRE, SSFP, or other rapid acquisition sequences such as echo planar imaging [2]. Ventricular volumes can be measured at end-diastole and end-systole using traditional area-length approaches from the long-axis images or using Simpson's rule with serial short-axis images [3]. Simpson's rule is the common method of computing volumes of continuous objects by summing the areas of cross sections obtained at a discrete number of points. While most current techniques acquire contiguous slices, gaps between sampled cross sections are treated as if they were represented by the average of the nearest cross-sectional views. In essence, the area is found by summing each cross-sectional area and multiplying it by the sum of the slice thickness and the interslice gap. Stroke volume and ejection fraction can be readily determined from the end-systolic and end-diastolic volumes. In addition to the geometrically simple left ventricle, the more irregularly shaped right ventricle can also be studied using a Simpson's rule approach with serial short-axis views from base to apex. The three-dimensional coverage of CMR images makes possible calculation of highly accurate right ventricular volumes and ejection fractions [4]. By evaluating size, shape, and the regional contractile ability of the left ventricle, lesions such as ventricular aneurysm and pseudoaneurysm, dilated and hypertrophic cardiomyopathy, myocardial thinning, and remodeling can readily and comprehensively be evaluated. CMR is the most reliable means for assessing right and left ventricular

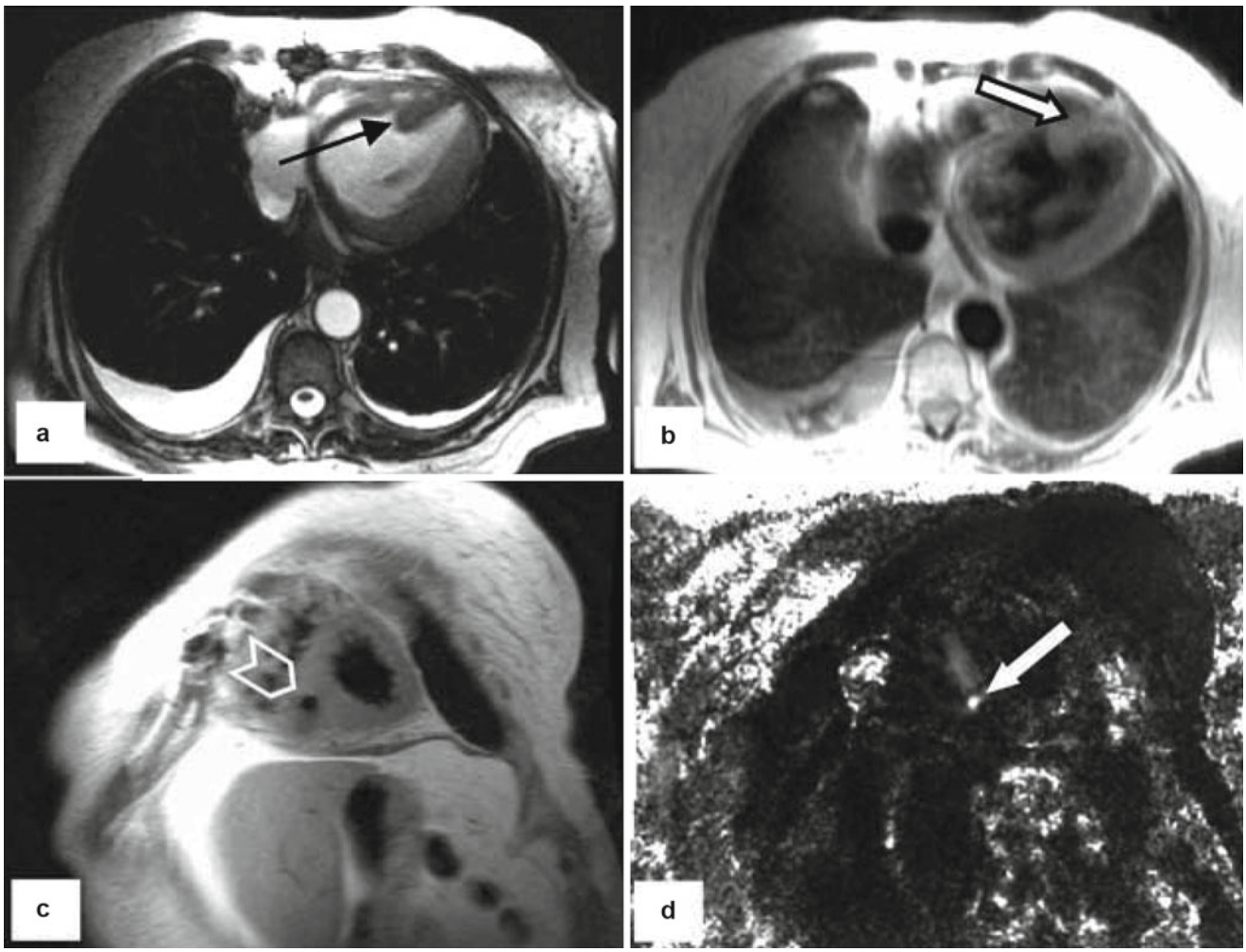

Fig. 13.3 A 54-year-old female with progressive dyspnea 6 month following an anterior septal MI. A murmur was heard prompting an MRI evaluation. (**a**) A septal defect in the interventricular myocardium is seen (*arrow*). (**b**) The high-velocity flow between the LV and RV was diagnostic of a post-infarct VSD (*arrow*). (**c**) Selective breath-hold imaging reveals the distinct septal hole (*arrow*), allowing for measurement. (**d**) Phase velocity imaging allowed quantitation of the Qp:Qs of 2.2, primarily left to right. As the patient was turned down for surgical repair, she underwent compassionate use of the nonsurgical ASD closure device for the VSD (*arrow*)

function. Since the myocardium is clearly visualized, it is easy to measure wall thickness and to evaluate wall thickening [5]. Furthermore, global and regional myocardial mass can be measured [6].

In addition to functional evaluation with conventional contrast imaging, other methods specific to cardiovascular MR studies are available: phase velocity mapping and RF tagging. Phase velocity mapping is analogous to Doppler echocardiography. In phase velocity mapping, the phase of each pixel in the MR image is related to the voxel's velocity. Unlike Doppler echocardiography, it is not dependent on exact angulation, and it measures velocity and flow accurately in two and as many as three dimensions. Phase velocity mapping has a plethora of applications, including blood flow visualization and determination of stroke volume and cardiac output at the aortic valve and in evaluating ventricular septal defects (Fig. 13.3). Shunt flow may be evaluated by comparing aortic flow to pulmonary artery flow. RF tagging provides CMR with a unique ability to more precisely evaluate regional myocardial function [7]. By using the appropriate perpendicular saturation band pulse sequence, dark lines in a regular crisscross pattern can be applied to the myocardium at the time of the ECG R wave. Since these lines move with the myocardium, intrinsic motion can be visualized to assess true function without the confounding effect of myocardial through-plane motion [8] or remote muscle influences (tethering). Furthermore, changes in distance between intersections of RF grid lines can be tracked and regional strains, indices of rotation, and translation amounts calculated. Unlike tracking of material markers, RF tagging does not impede or influence myocardial dynamics, and it is completely noninvasive.

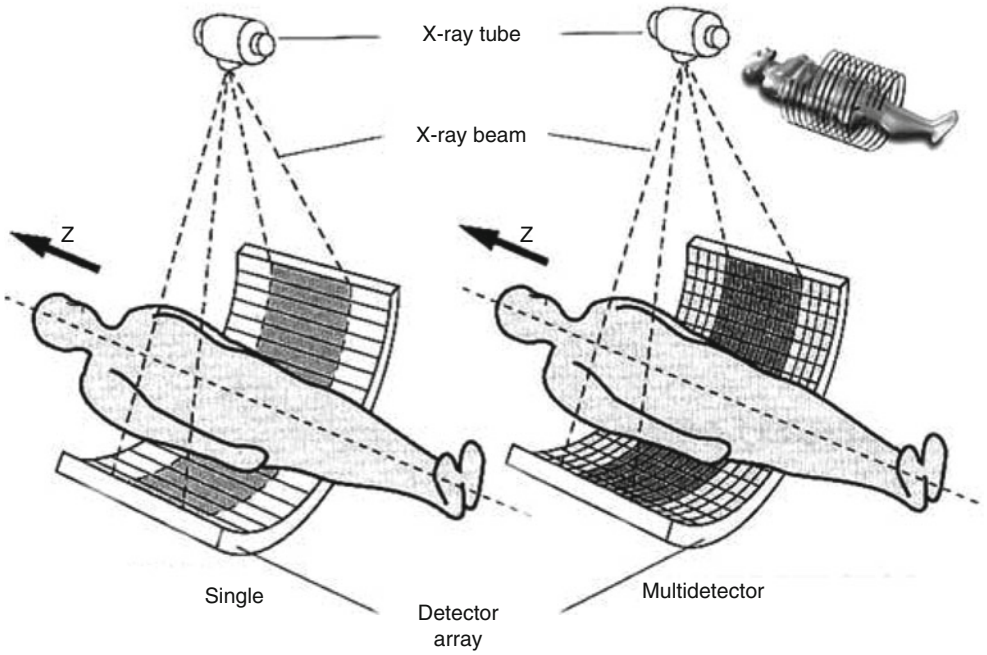

Fig. 13.4 Multidetector CT. Comparison of single-slice and multidetector CT. Multidetector CT uses an array of detectors to improve resolution (smaller pixels) and temporal (more slices) coverage of the heart and great vessels. Cardiac CT has shown continued improvement as detector arrays have increased from 1 to 2, 4, 8, 16, 40, and 64

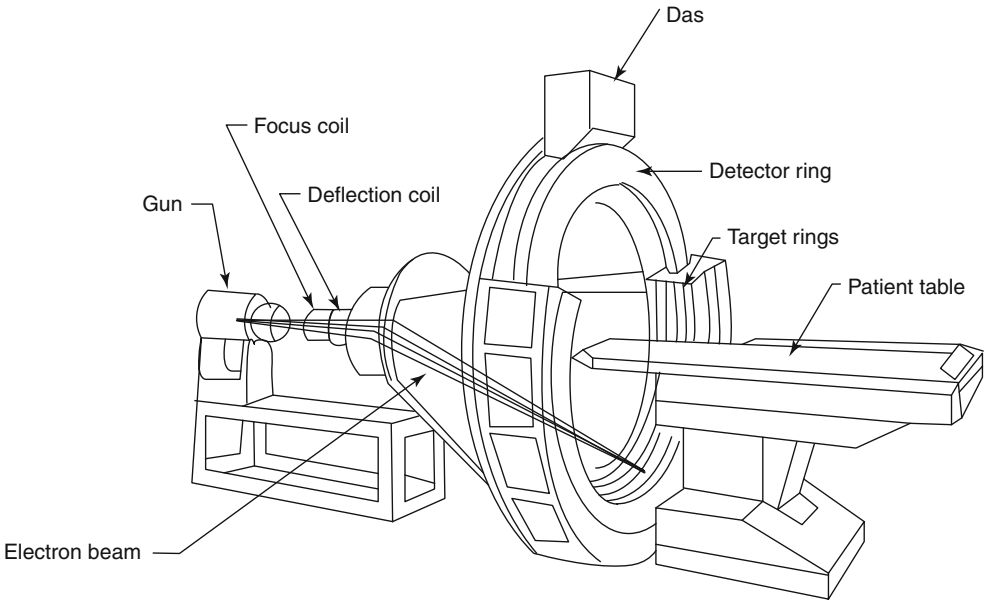

Fig. 13.5 Diagrammatic display of an electron beam computed tomographic imaging system (Courtesy of GE Healthcare)

Computed Tomography

The main type of CT systems used for cardiovascular diagnosis is multidetector CT (MDCT). MDCT devices use a slip ring, continuously rotating X-ray source, and circular arrays of stationary detectors (Fig. 13.4). MDCT is performed with the table continuously in motion during scanning, generating multiple (4, 8, 16, 32, 64, 125, 256 up to 320) spiral slices per 250–400 ms revolution, with excellent ($<0.5 \times 0.5 \times 0.5$ mm^3) spatial resolution. MDCT cardiac acquisitions must be ECG-triggered and coupled with a breath hold between 1 and 10 s. Partial rotational data may be subsegmentally reconstructed to produce cardiac images with an effective temporal resolution for MDCT images from 50 to 200 ms (Fig. 13.5).

Cardiovascular CT spatial resolution is considerably better than MR. Single-source MDCT is difficult to perform effectively in patients with a heart rate over 90 beats/min. Heart rate reduction using a β-blocker such as propranolol (20–40 mg) or metoprolol (50–100 mg) prior to MDCT for coronary artery examinations is desirable [9]. Currently available MDCT techniques allow for better control of the X-ray tube output to reduce radiation exposure. However, MDCT does not spare the radiation exposure compared to angiography. When angiographic intervention procedures are performed, they generate considerably more radiation exposure for patients and personnel [10, 11].

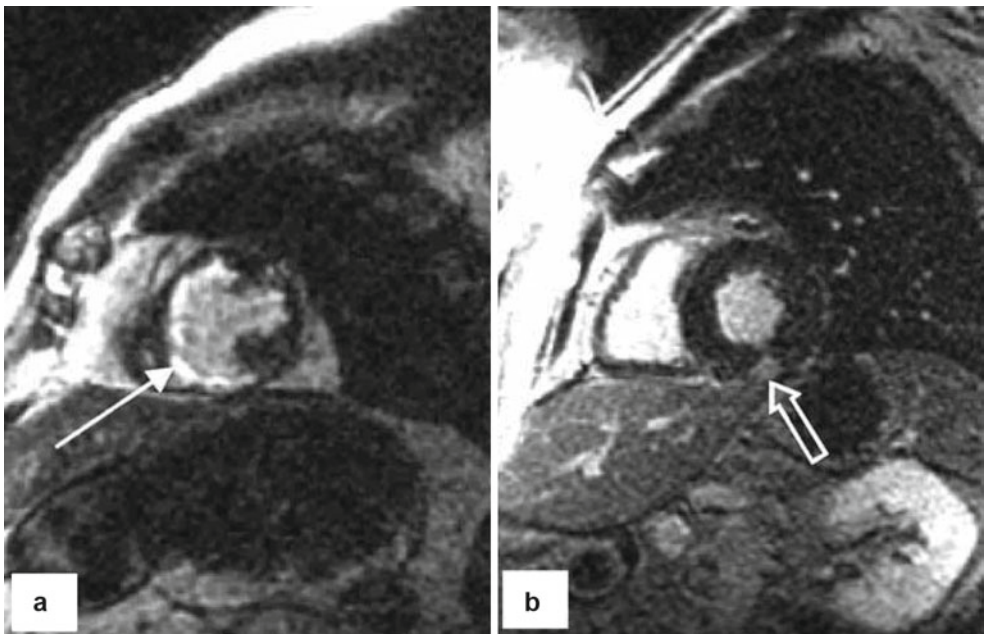

Fig. 13.6 A paramagnetic agent (gadolinium DTPA) was infused and the delayed enhancement image seen here acquired after a delay of 15 min. The accumulation of gadolinium is seen (*arrows*) indicating distribution of necrotic myocardium. (**a**) A large region is affected. (**b**) A small region is affected in a patient with equivocal troponin I (7 ng/dL). The latter patient underwent cardiac catheterization, demonstrating a left circumflex distal marginal occlusion

Because the relative radiographic densities of the myocardium and the blood pool are nearly identical, other than for the evaluation of coronary artery calcification, there is an absolute need to administer iodinated radiopaque contrast medium with CT [12]. Some patients may be allergic to radiopaque contrast media, and administration of contrast medium could precipitate renal failure in patients with borderline renal function or idiosyncratically in those with normal function. Finally, the osmotic load required to generate important diagnostic information could precipitate an episode of pulmonary edema in patients with congestive heart failure. The use of low-osmolality nonionic contrast agents is required in such patients but does not reduce the incidence of renal impairment.

CT Methods

A number of recent studies have described the use of MDCT to assess right and left ventricular function. These are typically acquired in a continuous series over several heartbeats, a process known as retrospective acquisition. After intravenous administration of radiopaque contrast medium, serial images depict the cardiac chambers with good contrast between ventricular wall and ventricular blood pool. From such an acquisition, left and right ventricular volume and ejection fraction can accurately be determined. Like CMR, MDCT provides a means of evaluating heart function, including chamber volumes, ejection fraction, and myocardial mass. Unlike CMR, it is essential to use radiopaque contrast medium to define the endocardial borders of the cardiac chambers. High-resolution images can be generated that allow precise measurement of regional and global ventricular function at the expense of higher doses of effective radiation compared to prospectively ECG-triggered MDCT acquisition. As with CMR, a series of short-axis ventricular slices can be reconstructed from the volumetric data and ventricular volumes calculated. These slices can sample 10–20 or more images throughout the cardiac cycle depending on the baseline heart rate and temporal resolution of the CT scanning hardware. With a modification of Simpson's rule, ventricular volume and mass can be determined. Studies in both laboratory animals and humans demonstrate the reliability of left ventricular volume and mass determination using MDCT. Similar results have been demonstrated previously using EBCT.

Ischemic Heart Disease

Since CMR and MDCT can reliably evaluate the function of both ventricles by examining volumetric changes and changes in myocardial thickness during systole and diastole, they can be used to demonstrate regional wall motion abnormalities [13]. Using gadolinium MR contrast agents, one can see delayed hyperenhancement of the infarcted myocardium (Fig. 13.6) [14, 15]. Unlike nuclear or echocardiographic techniques, this seems to be a unique phenomenon of CMR and presently is the subject of intense research. Specifically, the extent of delayed enhancement, or "transmurality," has been shown to be predictive of functional recovery after appropriate revascularization. Further prognostic value can be attained by the evaluation of microvascular obstruction within

a prior myocardial infarction, a process also known as "no reflow" on traditional coronary angiography [16] (Fig. 13.7).

Myocardial *ischemia* can be diagnosed by comparing resting images obtained at rest to images acquired after approaches that increase myocardial blood flow, such as handgrip, pharmacologic infusion of dobutamine or of a vasodilator agent, or even exercise using specialized equipment [17]. Coronary vasodilator agents such as regadenoson, adenosine, and dipyridamole may be infused during contrast-enhanced CMR perfusion studies to demonstrate reduced dynamic enhancement in territories served by stenotic coronary arteries (Fig. 13.8) [18]. The imaging and physiologic principles are similar to those of radionuclide or "nuclear" perfusion stress testing [19, 20].

Using CMR cine, one sees deterioration in left ventricular myocardial contraction with higher doses of dobutamine in segments supplied by coronary arteries with significant stenoses. Myocardial *viability* can also be assessed through a phenomenon termed "contractile reserve" when dobutamine stress CMR is used to enhance poorly contracting myocardial segments. One would see improvement in wall motion with low-dose dobutamine but deterioration of the wall motion of the same segments at higher doses due to ischemia, that is, the biphasic response, in the presence of viable but hypocontractile myocardium.

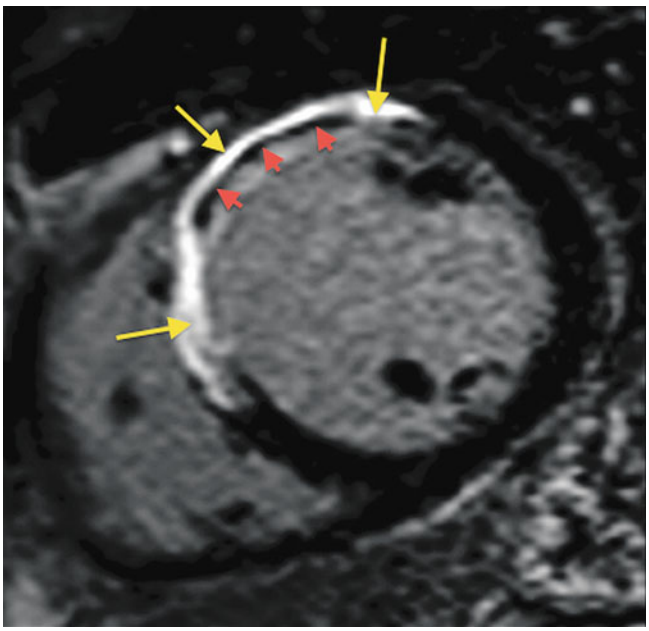

Fig. 13.7 Delayed enhancement image in a short-axis view of the mid-left ventricular cavity demonstrating transmural delayed gadolinium enhancement in the anterior and anteroseptal walls consistent with a left anterior descending coronary artery myocardial infarction (*yellow arrows*). The area of reduced signal within the core of the infarct represents microvascular obstruction, analogous as "no reflow" on coronary angiography (*red arrows*)

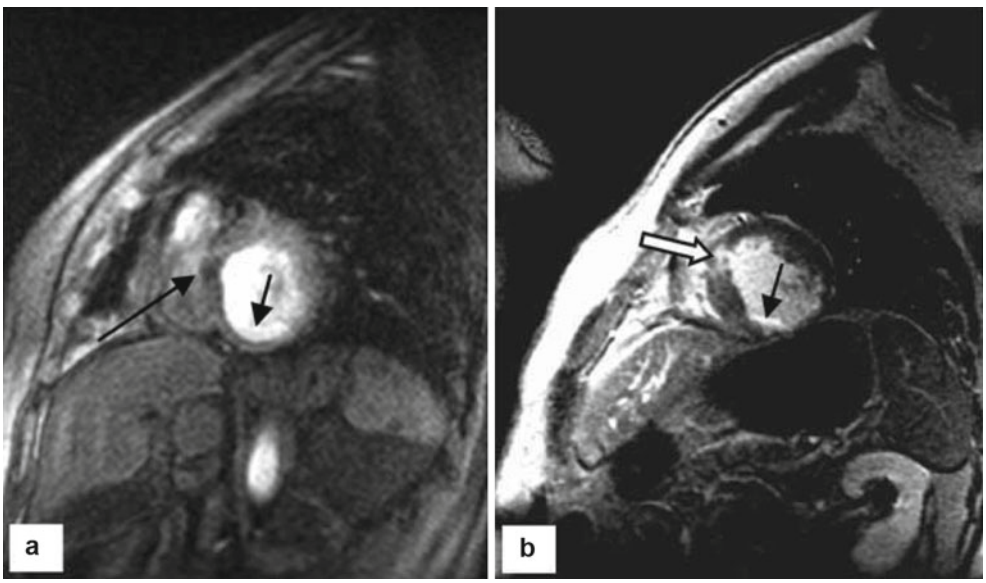

Fig. 13.8 (**a**) FSGRE image of a short-axis slice demonstrating the concept of first-pass perfusion using gadolinium. The *large arrow* indicates a focal hypoenhanced near-transmural anteroseptal lesion, representing the relative lack of gadolinium's T1 effect in poorly perfused myocardium (low signal) as compared to the otherwise normally perfused myocardium (higher signal). The *small arrow* points to a small endocardial lesion missed by nuclear imaging due to its 1–2 mm thickness, well below the 10–13 mm resolution required for radionuclide-based techniques. (**b**) A unique property of CMR, using this technique, is the relative late (5–20 min) effect that contrast provides to highlight necrotic (scarred) myocardium, *outlined arrow*. As shown in the *small arrow*, an even smaller endocardial scar can be seen, partially encircling the inferior/inferior lateral wall. This technique, referred to as "delayed hyperenhancement," is now demonstrated to be the reference standard for interrogation of myocardial viability

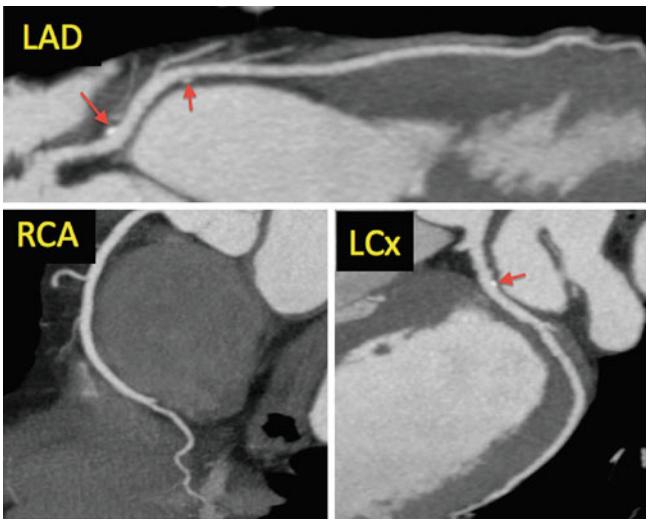

Fig. 13.9 Coronary CT angiogram depicting mild, non-obstructive calcified plaque in the proximal and mid-LAD and proximal LCx (*red arrows*). The RCA and PDA appear widely patent and are free of coronary atherosclerosis. *LAD* left anterior descending coronary artery, *LCx* left circumflex coronary artery, *RCA* right coronary artery, *PDA* posterior descending coronary artery

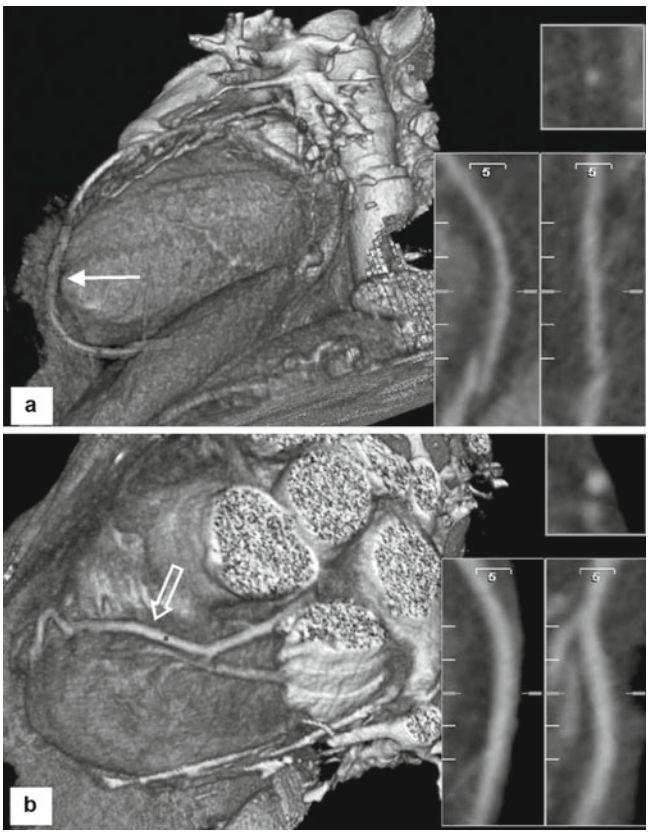

Fig. 13.10 Images obtained using MDCT processed to highlight the LAD and epicardium. (**a**) Distal view (*arrow*) and (**b**) the proximal section (*arrow*). Inserted views depict orthogonal views of the highlighted sections

CT approaches to myocardial perfusion can be applied to semiquantitatively assess perfusion levels [21]. By analyzing the myocardium as the contrast agents perfuse it, it is possible to calculate regional perfusion using automated software evaluation of myocardial segments similar to that currently performed by nuclear perfusion studies. CT perfusion with vasodilator stress has been shown to be feasible and safe and have good correlation to SPECT and CMR perfusion [22–24].

Coronary Artery Imaging

In many instances, visualization of the coronary arteries is required, and substantial progress in both techniques, but particularly MDCT has been made toward this goal during the past decade.

Currently, MDCT is able to routinely visualize normal coronary arteries using multidetector technology (initially attempted with 16 and 32 slice systems) and more recently using 64, 128, 256, and 320 slice detector systems. Rapid advancements in this field coupled with advanced acquisition techniques have led to the widespread adoption of MDCT as the gold standard noninvasive evaluation of coronary artery disease. Several multisite studies have demonstrated the overall very high negative predictive value (>99 %) of this technique in individuals with low to intermediate likelihood of coronary disease. An example of a coronary CT angiogram with mild, non-obstructive calcified plaque (red arrows) in the proximal LAD and LCx is shown in Fig. 13.9 (LAD, left anterior descending; LCx, left circumflex; RCA, right coronary artery). Exciting new developments in this field include the ability to integrate flow information through computational fluid dynamics, permitting noninvasive evaluation of fractional flow reserve (FFR-CT). Limitations to MDCT still include contrast requirements, the need to administer β-blockers to reduce the heart rate to approximately 60 beats/min, and radiation doses. Improvements in spatial resolution may allow reductions in contrast dosage (Fig. 13.10b) [25]. Through various radiation dose-lowering techniques such as reduced tube voltage, greater use of prospective ECG-triggering, and iterative reconstruction, effective radiation doses have seen a dramatic decline since the introduction of 64-slice MDCT technology in 2004.

Using the latest instrumentation and MR techniques, imaging the proximal coronary trunks and some more distal segments of the coronary arteries is feasible. It has been shown to be more accurate for the delineation of anomalous coronary arteries than X-ray angiography (Fig. 13.11). Limitations of coronary MRA include long acquisition times (typically upward of 10 min), motion artifacts, and the intrinsic temporal and spatial resolution limits of the CMR system. Certainly, more investigation is needed to refine coronary MRA for it to be adopted in a widespread fashion. Such additions as the use

of a blood pool contrast agent might improve the sensitivity and specificity as compared with catheter coronary angiography. A few investigators have evaluated the potential for CMR to characterize coronary arterial plaque. Clinical determination of plaque vulnerability may be within the realm of possibility for this versatile technology.

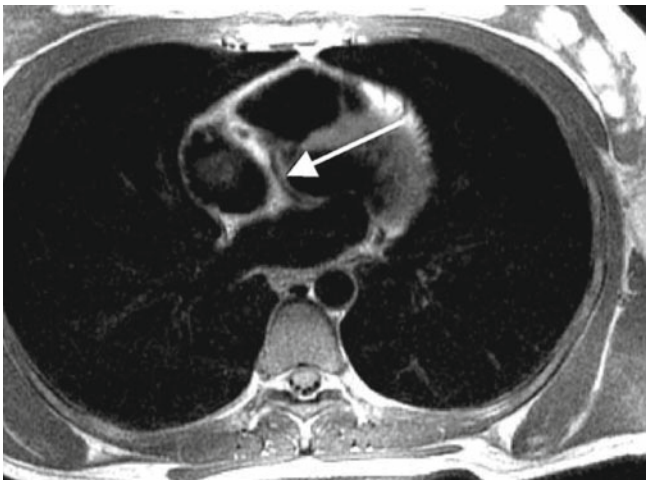

Fig. 13.11 This 45-year-old patient presented with chest pain, underwent X-ray coronary angiography, and was found to have an anomalous left circumflex arising off the right coronary sinus. Regarding the question as to trajectory, the catheterization results were equivocal, prompting a cardiac MRI. This double-inversion recovery image was acquired in a breath-hold manner without administration of contrast, clearly demonstrating the benign nature of this anomaly. The vessel travels posterior to the aortic root (*arrow*) as the great majority, if not all, of anomalous left circumflex vessels do

Coronary Calcium

Both MDCT and EBCT detect coronary artery calcification, as direct evidence of coronary atherosclerosis [26]. In view of the high speed of EBCT acquisition, the coronary arteries are virtually "frozen" in space, and the extent of calcification can be accurately assessed (Fig. 13.12). MDCT also can provide relatively fast imaging, but with 50–200 ms acquisitions, the blurring effect due to cardiac motion could be problematic, although less so with modern 64-slice or greater systems (Fig. 13.13). Because of the widespread availability of MDCT scanners, in contrast to EBCT scanners, it is important to note that MDCT provides coronary artery calcification scoring comparable to that of EBCT. Use of coronary artery calcification as a predictor of functionally significant coronary artery disease remains controversial [27], especially in younger individuals who have predominantly noncalcified plaque. It clearly indicates the presence and burden of atherosclerosis but not its physiologic significance. Proponents of the application of EBCT maintain that it should become a routine study for coronary risk assessment [28]. Others suggest that plaque rupture, a common cause of coronary occlusion, is related to the lipid constituents of plaque (invisible to X-rays), but not to the amount of calcium. At present, the value of the EBCT coronary calcium score is uncertain, and it does not supplant current clinical methodologies, although it does provide another, albeit expensive, means for risk assessment [29]. The most recent 2007 ACC/AHA Consensus Document supports the role of CT coronary calcium measurement in asymptomatic patients with intermediate coronary heart disease risk, that is, those at 10–20 % 10-year risk

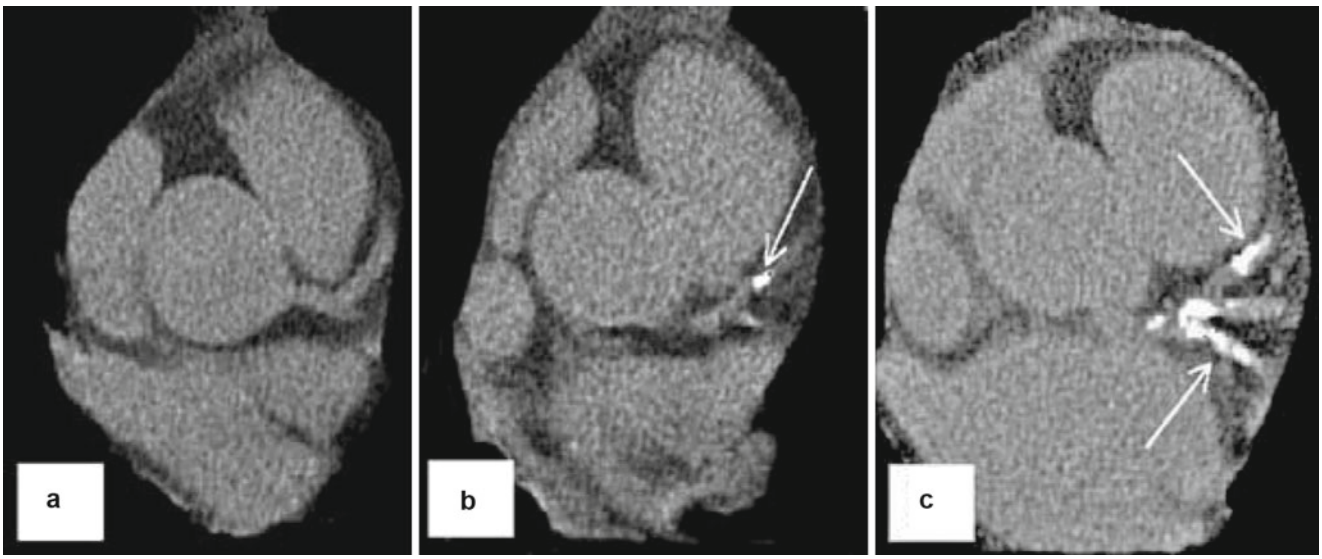

Fig. 13.12 Examples of progressive coronary artery calcification (**a–c**) depicting increasing signal as the intraluminal calcium burden rises. Formal calcium scores can be derived using the Agaston algorithm from the scans quantifying the signal from the calcium. Although calcium is a well-accepted marker for atherosclerosis, the direct relation between calcium and prediction of clinical events is less well established (Courtesy of GE Healthcare). *Arrows* represent calcified coronary artery plaque

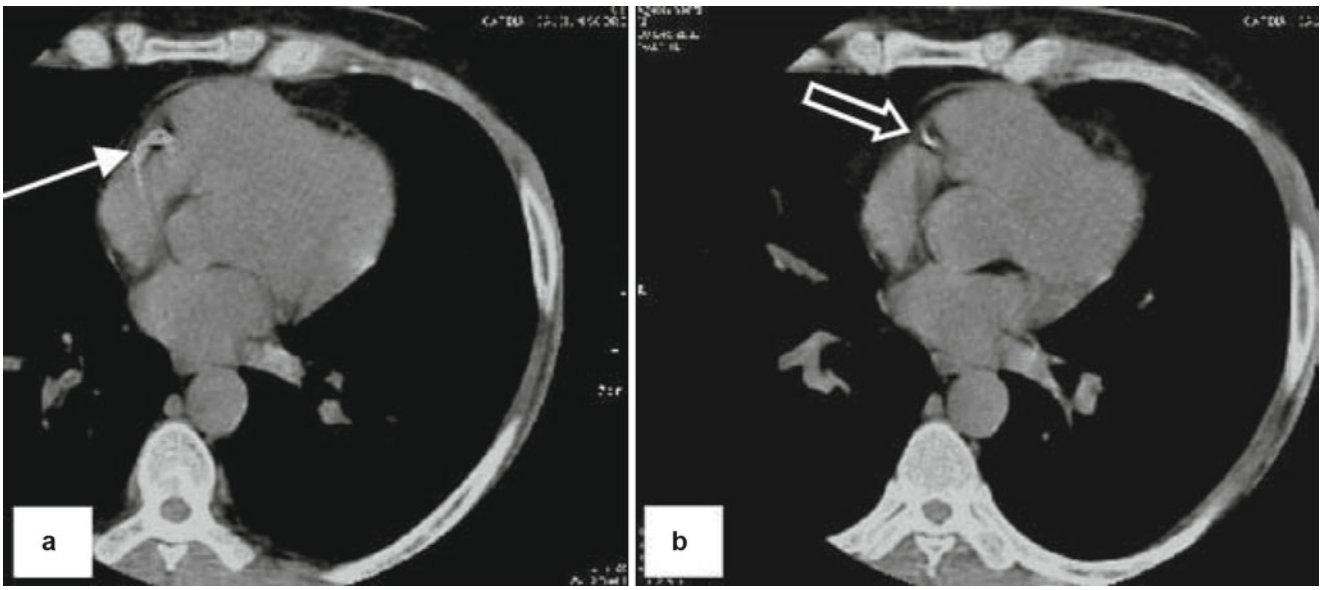

Fig. 13.13 Examples of low levels of coronary artery calcification (*arrows*, **a–b**) visualized as increased signal as the intraluminal calcium burden rises

of death or myocardial infarction (class IIb recommendation, level of evidence B) [30]. Further data will be required to determine its actual utility [31].

Cardiomyopathies

With dilated and valvular cardiomyopathy (either acquired or of congenital origin), one might expect to find both left and right ventricular involvement and homogeneously depressed left ventricular wall motion (Fig. 13.14). Hemochromatosis, an infiltrative cardiomyopathy whereby iron accumulates in the myocardium, can be readily diagnosed by CMR. The iron that is localized in the myocardium and the liver generates a characteristic signal dropout pattern so that the liver and, in part, the myocardium demonstrate very low signal. In *sarcoidosis*, one can visualize the granulomatous infiltrates with delayed gadolinium enhancement that may lead to ventricular dysfunction as well as local inflammation.

One cardiomyopathy that may be well characterized by CMR is arrhythmogenic myocardial dysplasia. In this condition, which is associated with life-threatening ventricular arrhythmias, the right ventricle is involved with fat infiltration and myocardial thinning. The fatty infiltrate shows up as a bright signal on black-blood spin-echo CMR (in about half of these patients) and regional wall motion dysfunction (in most patients) on gradient-echo or SSFP images, combined with signal nulling on T2-weighted images, confirming the presence of intramyocardial fat deposits (or transformation) (Fig. 13.15). Morphologic imaging can also be accomplished with CT [32].

Hypertrophic cardiomyopathy (HCM) is a genetic cardiomyopathy that causes myocardial hypertrophy in a variety of patterns. The hypertrophy can be readily imaged and quantified with CMR imaging. One particular type of HCM that can be challenging to detect with standard echocardiography is apical variant HCM (aka "Yamaguchi's disease") [33] (Fig. 13.16). CMR may avoid this problem because it is less operator dependent, is not subject to acoustic-window limitations, and has multiplanar capability and displays excellent soft-tissue contrast.

Finally, cardiac amyloidosis has several characteristic patterns of delayed gadolinium enhancement on CMR imaging studies and can be readily identified. Interestingly, the development of myocardial gadolinium deposition predates any clinical manifestation and thus permits identification even in asymptomatic individuals.

Fig. 13.15 A 34-year-old woman presenting with several episodes of syncope and near syncope before a catheter-based electrophysiological study. The patient's risk was stratified using CMR. (**a**) A four-chamber view with *arrow* pointing to a mid-systolic asynergic, tardykinetic zone of the right ventricle free wall with thinning, meeting two major working group classifications for arrhythmogenic right ventricular dysplasia (ARVD). The third classification (out of four) is met in (**b**) as shown by a triple-inversion recovery sequence, a unique sequence to magnetic resonance, that takes advantages of the faster relaxation of fat compared to protein. This T2-weighted image provides insight into specific tissue characteristics, which is another important property of CMR. Note the subtle but evidence of fat within the myocardium corresponding to the asynergic zone. The fat signal of the breast tissue is similar to that within the affected RV free wall (*arrow*). The patient was referred to the NIH-sponsored ARVD trial and likely for defibrillator placement, the current standard for treatment

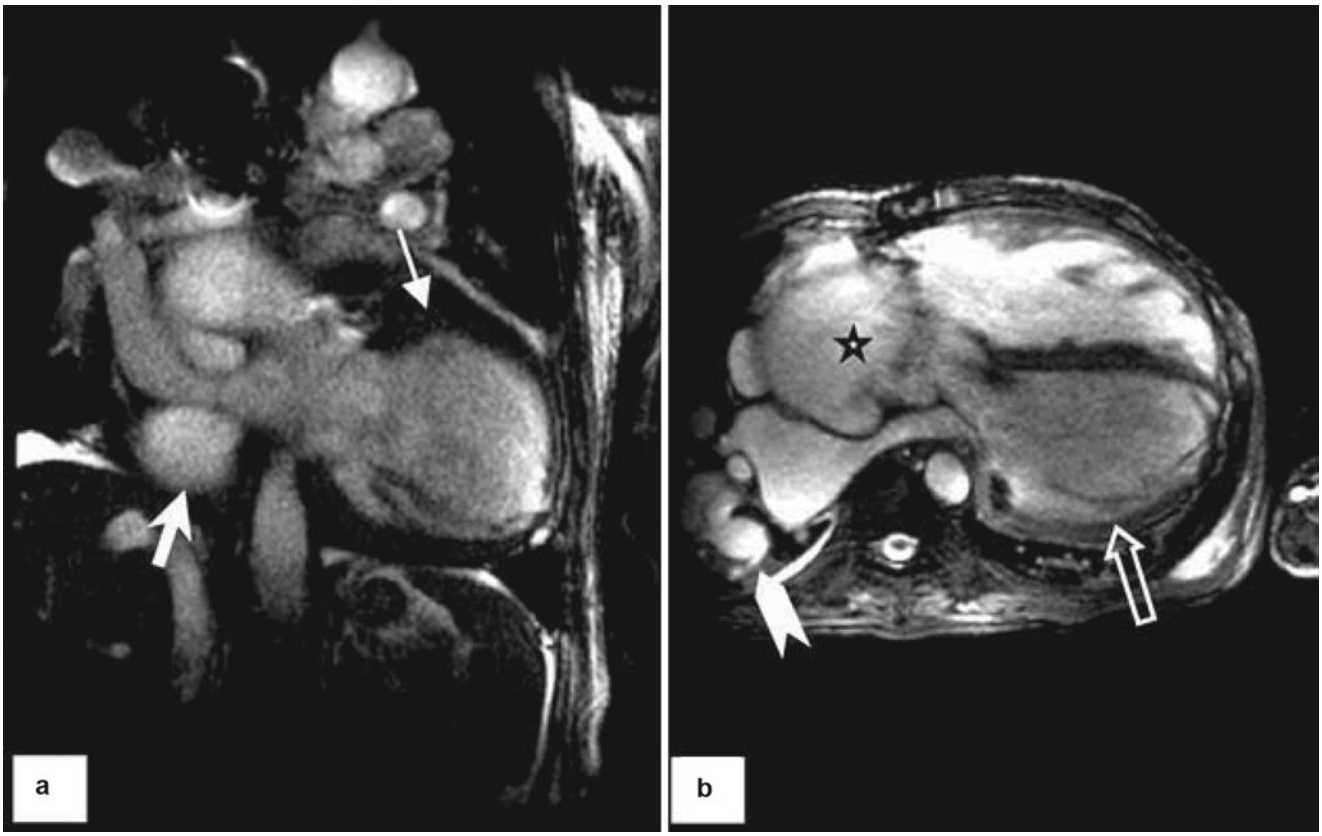

Fig. 13.14 A 32-year-old female presented 25 year after repair of tetralogy of Fallot. (**a**) The LV was dilated (*small arrow*), measuring 100 mm × 53 mm with a markedly compressed LA (*large arrow*). (**b**) Note the enlarged right ventricle, left ventricle (*open arrow*), and the RA/LA, as well as small aortobronchiolar communications to augment pulmonic flow (*chevron*). The enlarged aortic root (*star*) is probably related to late correction and high early childhood systemic flow due to redirection of pulmonic flow. Poor migration of neural crest cells with their elastin, forming progenitor cells, has been implicated in the aortic root and ascending aortic dilation, as seen in this patient who was shown to have a small contained aortic dissection (not shown)

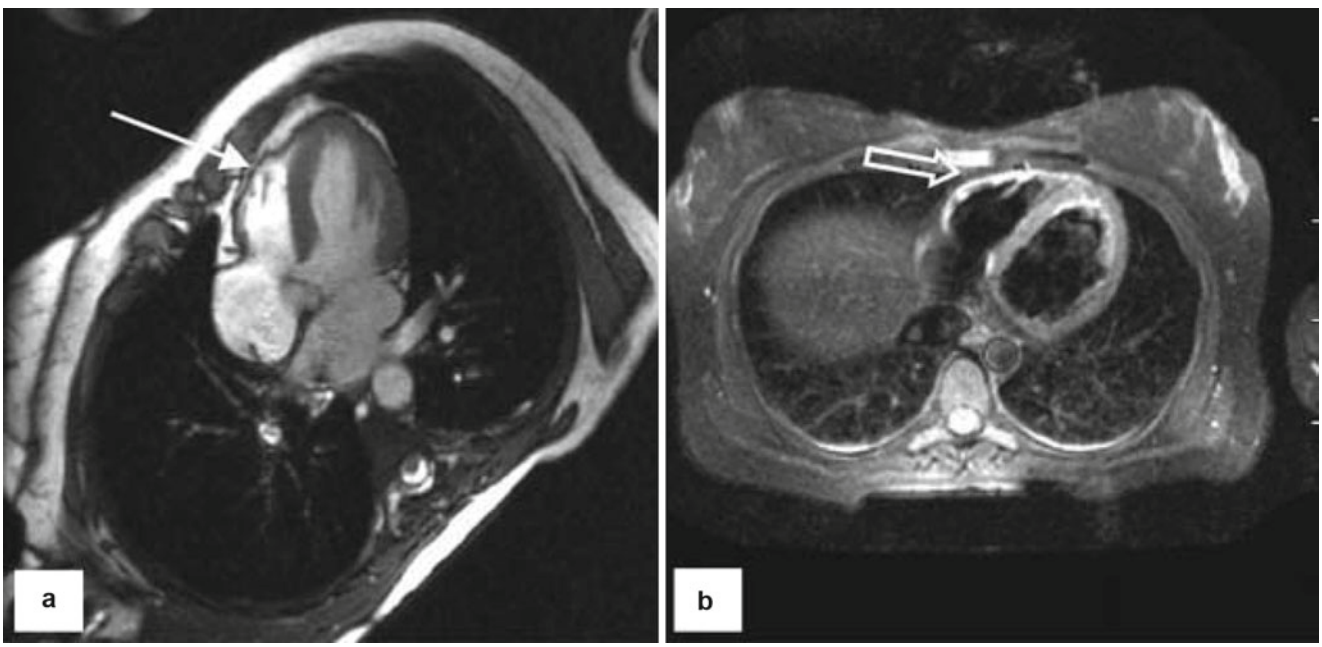

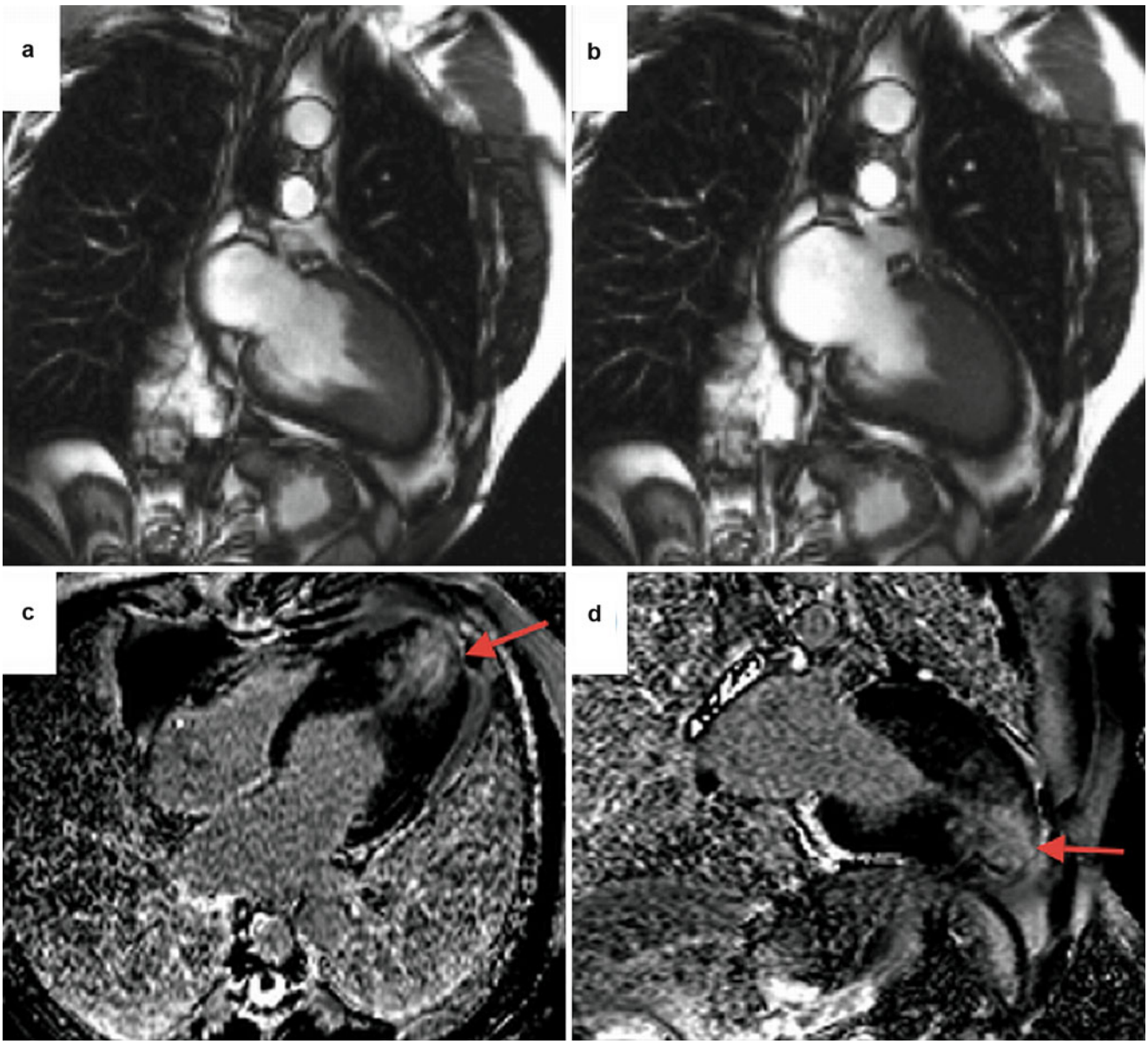

Fig. 13.16 A 42-year-old man presented with suspicion of apical hypertrophy on an echocardiogram. (**a**) SSFP cine sequence at end-diastole demonstrates apical hypertrophy and a "spade-shaped" ventricle, (**b**) SSFP cine at systole, and (**c** and **d**) phase sensitive inversion recovery delayed enhancement sequence showing marked apical enhancement (*red arrows*) consistent with apical variant of hypertrophic cardiomyopathy

Aortic and Peripheral Vascular Imaging

MRA offers excellent noninvasive imaging of the aorta, pulmonary arteries and veins, cerebral vasculature, and the iliofemoral arterial system. Satisfactory visualization of the lower extremity runoff vessels is routinely achievable. Because signal can be generated through the motion of blood, MRA may not require any contrast agent administration for many of these examinations. MR contrast agents have an excellent safety profile and are safe to use in patients with renal failure. The osmotic load is less than that of iodinated contrast agents. Intravenous contrast-enhanced MRA is routinely used for examinations of the aorta, pulmonary vessels, carotid arteries, renal arteries, and arteries of the lower extremity but can be performed in their entirety without contrast through time-of-flight approaches.

MRA of the aorta is considered to have equivalent sensitivity but superior specificity to transesophageal echocardiography or multislice contrast-enhanced CT for the evaluation of aortic aneurysms and aortic dissection. In dissection, intimal flaps and entry site can be identified, allowing for identification of the true and false lumen, differentiation between blood flow and clot in the false lumen, and involvement of branch vessels (Fig. 13.17). The critical distinction

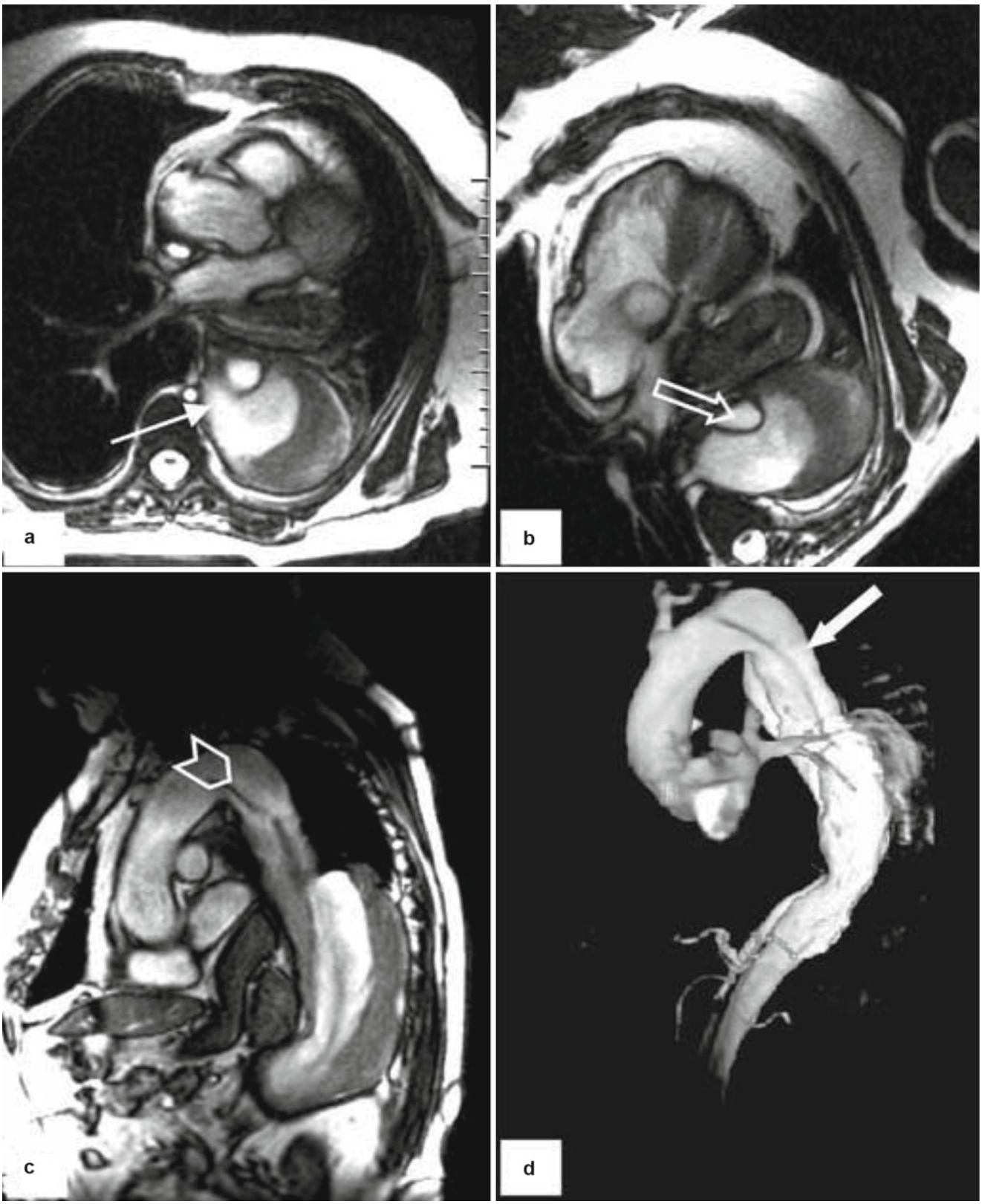

Fig. 13.17 Dissection and thrombus is visible in the false lumen. Multiple views of a type B descending aortic dissection are shown. (**a**) A SSFP axial slice depicts flow in the false lumen (*arrow*). (**b**) The partially thrombosed false lumen can be seen to the right (dark) and the true lumen is seen to the left (*arrow*). (**c**) The high descending aortic origination of intimal flap is seen (*chevron*). (**d**) A 3-D surface rendering of an MRA acquired in 22 s with gadolinium demonstrates the intimal flap (*arrow* indicates false lumen). Note the tiny true lumen in the abdominal aorta. The images demonstrate a "clean" dissection of the aorta with the true lumen supplying the right renal artery and the false lumen supplying the left renal artery

between DeBakey dissection type 1 or 2 and type 3 lesions is readily made with MR. Congenital anomalies of the aorta can also be identified, such as coarctation, arch interruption, and transposition. Imaging the cerebral arterial supply, including the carotid and vertebral arteries, has become routine in clinical practice, supplanting X-ray angiography.

The thoracic and abdominal aorta can readily be evaluated using MDCT after a bolus injection of radiopaque contrast medium. Aortic aneurysms and dissections are detected and assessed. Where CMR is not available, MDCT, EBCT, or TEE are preferred for diagnostic assessment. Like CMR, CT methods are useful for visualizing the intimal flap and for determining the extent of branch vessel involvement. CMR and CT are useful for differentiating between aortic aneurysm with mural thrombus and dissection with thrombus in the false lumen.

Both MDCT and EBCT have been used to visualize the renal arteries in the evaluation of hypertensive patients with suspected renal artery stenosis. Using contrast enhancement patterns, kidney volumes (both cortical and medullary) can be determined. High-speed CT provides a means of examining renal blood flow and excretion. Branch vessels from the aorta can also be well visualized, including the carotids and vertebral arteries, the trifurcation, the celiac, the superior and inferior mesenteric, the brachiocephalic, the iliofemoral, and the popliteal arteries. CMR is the preferred technique in the majority of patients, especially if there is evidence for renal compromise. One caveat to this rule is when severe baseline chronic kidney disease is present (estimated glomerular filtration rate <30 mL/min). In this situation administration of gadolinium chelates has been reported to rarely lead to nephrogenic systemic fibrosis, a chronic, progressive, and debilitating condition associated with cutaneous, subcutaneous, and joint thickening and fibrosis with resultant disability and immobility [34].

Pulmonary Arteries

Pulmonary emboli have been reliably identified using MDCT, which requires breath holding for optimal imaging of the pulmonary arteries. For patients with possible pulmonary embolism, breath holding is a very difficult challenge. EBCT, however, requires no breath holding. Both breath-hold MDCT and non-breath-hold EBCT have been reported to have sensitivity on the order of 85 % and specificity in the low 90 % range, in a select group of patients with intermediate probability of pulmonary embolism by radionuclide ventilation-perfusion scanning. Generally, the combination of ventilation-perfusion scanning followed by CT is the optimal strategy for detecting pulmonary embolism in a minimally invasive way. CT, like MR, is also very useful for the evaluation of pulmonary veins for anomalies and thrombosis. MRI has been used in limited manner for pulmonary embolism evaluation, although is ideal for pulmonary arteriovenous malformations (Fig. 13.18).

Valvular Disease

CMR can demonstrate valve anatomy, leaflet motion, and blood flow. Regurgitant or stenotic valves appear as regions of signal loss, due to the dephasing of spins within the jet of disturbed flow, on bright-blood cine MR images (Fig. 13.19). Regurgitant lesions may be evaluated by the size of the signal void (for a given TE), the volume of the accepting chamber, the time over which the signal void persists, and the size and duration of persistence of the zone of proximal convergence (i.e., the region where blood converges radially toward the valve orifice) [35].

The severity of valve disease may also be quantitatively evaluated with *phase velocity mapping*. This is similar to Doppler echocardiography. Phase velocity images are related to the velocity of spins passing through a given plane. Phase velocity mapping can be used to quantitate the flow rate volume and velocity of the blood. Stenotic valvular lesions are frequently characterized by phase image velocities as high as or even higher than 8 m/s (i.e., any velocity encountered in human valvular heart disease). Using a modified Bernoulli approach, pressure drop in mmHg may be estimated from phase contrast-measured velocities:

$$\text{Pressure drop} = 4 \times \text{velocity}^2$$

Thus, CMR can be used to assess both regurgitant and stenotic valvular disease. However, its ability to directly visualize normal valve tissue and associated abnormalities, such as endocarditis, while improving, may be somewhat limited compared with echocardiography. It is possible, however, to make excellent images of a bicuspid or tricuspid aortic valve.

Cardiac Masses

Clearly, intracardiac masses such as atrial myxomas and atrial and ventricular thrombi can be detected and evaluated by CMR or MDCT. In fact, ventricular thrombi have been shown to be detected with higher sensitivity and specificity by CMR than by TEE. Virtually any tumor within the heart or that compromises atrial or ventricular function can be assessed. Unfortunately, rhabdomyomas and fibromas may not be distinguished from myocardium on CT, since their density is equivalent to that of myocardium. Differential dynamic contrast enhancement may be useful here. However, because of its sensitivity to T1 and T2 parameters, CMR can frequently differentiate tumors from myocardium (Figs. 13.20, 13.21, 13.22, 13.23, 13.24, and 13.25).

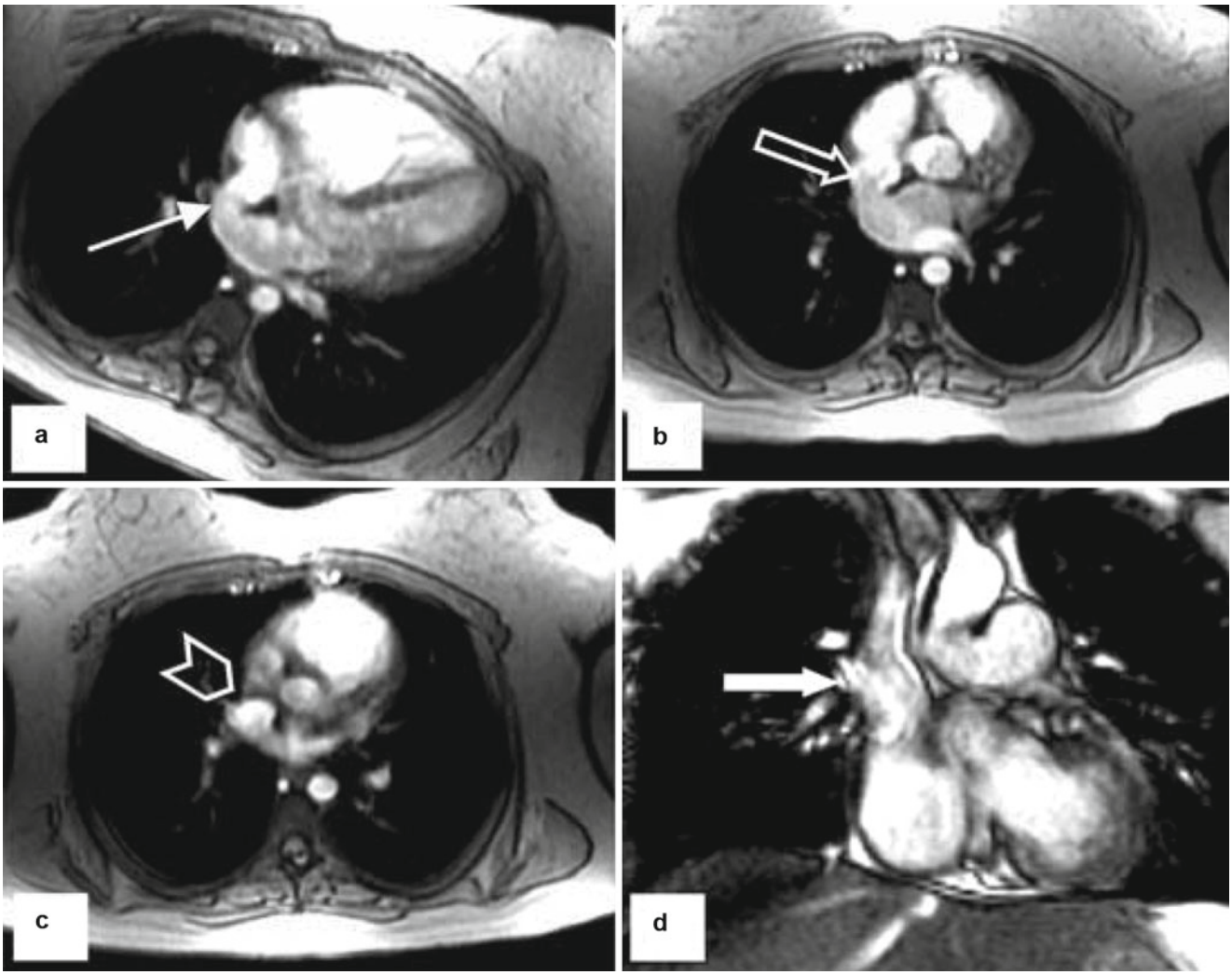

Fig. 13.18 A 24-year-old female presented to the internal medicine clinic for establishment of routine care. A murmur was heard and an echo performed, demonstrating normal LV/RV size, no intracardiac shunt, and an atypical posterior RA signal by color Doppler, prompting a cardiac MRI. (**a**) Demonstrates an absent posterior inner atrial septum with flow saddling between the RA and LA. The "broken ring sign" is present in **b** (*arrow*) demonstrating the classic sinus venosus defect as a defect between junction of the low SVC and high RA, a less common form of an ASD with an obligate anomalous right upper pulmonary vein. (**c**) Demonstrates the defect in the posterior RA (*arrow*). (**d**) Demonstrates the anomalous entry of the right upper pulmonary vein into the SVC/RA junction (*arrow*), confirming, on a second oblique, the presence of the congenital defect. Phase velocity mapping was performed demonstrating a Qp:Qs of 1.7 and a top normal RV size (115 mL) indicating a hemodynamically significant intracardiac shunt, worthy of repair, which was successfully conducted noninvasively

Pericardial Disease

CMR can readily visualize, measure, and characterize (i.e., distinguish transudate from exudate) pericardial effusions. The problem of differentiating between constrictive pericarditis and restrictive cardiomyopathies is made easier by using MR methods, since the pericardium can be visualized and its thickness measured (*see* Fig. 13.23) [36]. Adherence between the visceral and parietal pericardia, the equivalent of surgical visualization of adhesions, is possible employing RF tissue tagging. Under normal circumstances pericardial thickness should not exceed 3 mm. Restrictive left ventricular filling can be demonstrated by volumetric analysis using CMR or by phase velocity mapping. Finally, late gadolinium enhancement of the pericardium is a pathognomonic feature of acute pericarditis (Fig. 13.26).

The pericardium can be visualized by CT techniques as a thin layer, from 1 to 2 mm thick, with density similar to that of myocardium. As with CMR, pericardial thickening can readily be visualized by MDCT and EBCT, although the contrast between pericardium and myocardium may be better on CMR. While pericardial disease should be evaluated by two-dimensional echocardiography and Doppler approaches, both CMR and CT methods are useful for more comprehensive evaluation of patients with possible pericardial disease. CT is clearly the optimal technique to detect pericardial calcification.

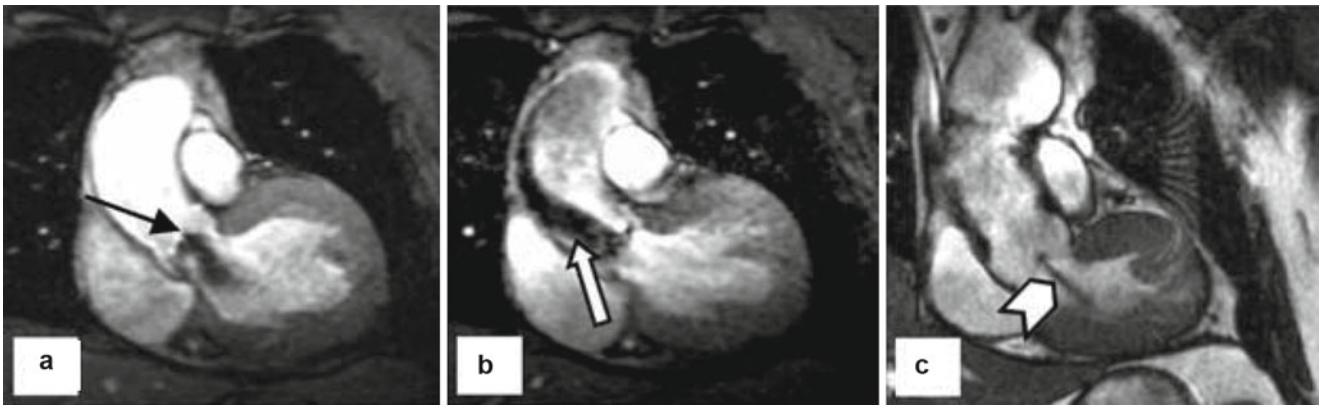

Fig. 13.19 Aortic regurgitation and aortic insufficiency. A 65-year-old male with combined aortic valvular lesions. (**a**) Central aortic regurgitation (*arrow*) and (**b**) the dephasing jet of an aortic stenosis (*arrow*). A moderately thickened, calcified, and restricted aortic leaflet is seen by SSFP imaging. Phase velocity mapping (not shown) quantified mean and peak gradient of 45–87 mmHg, respectively, confirming the diagnosis of severe aortic stenosis with moderate aortic regurgitation. (**c**) A mild jet of aortic regurgitation in another patient with an interposed tube graft (*chevron*)

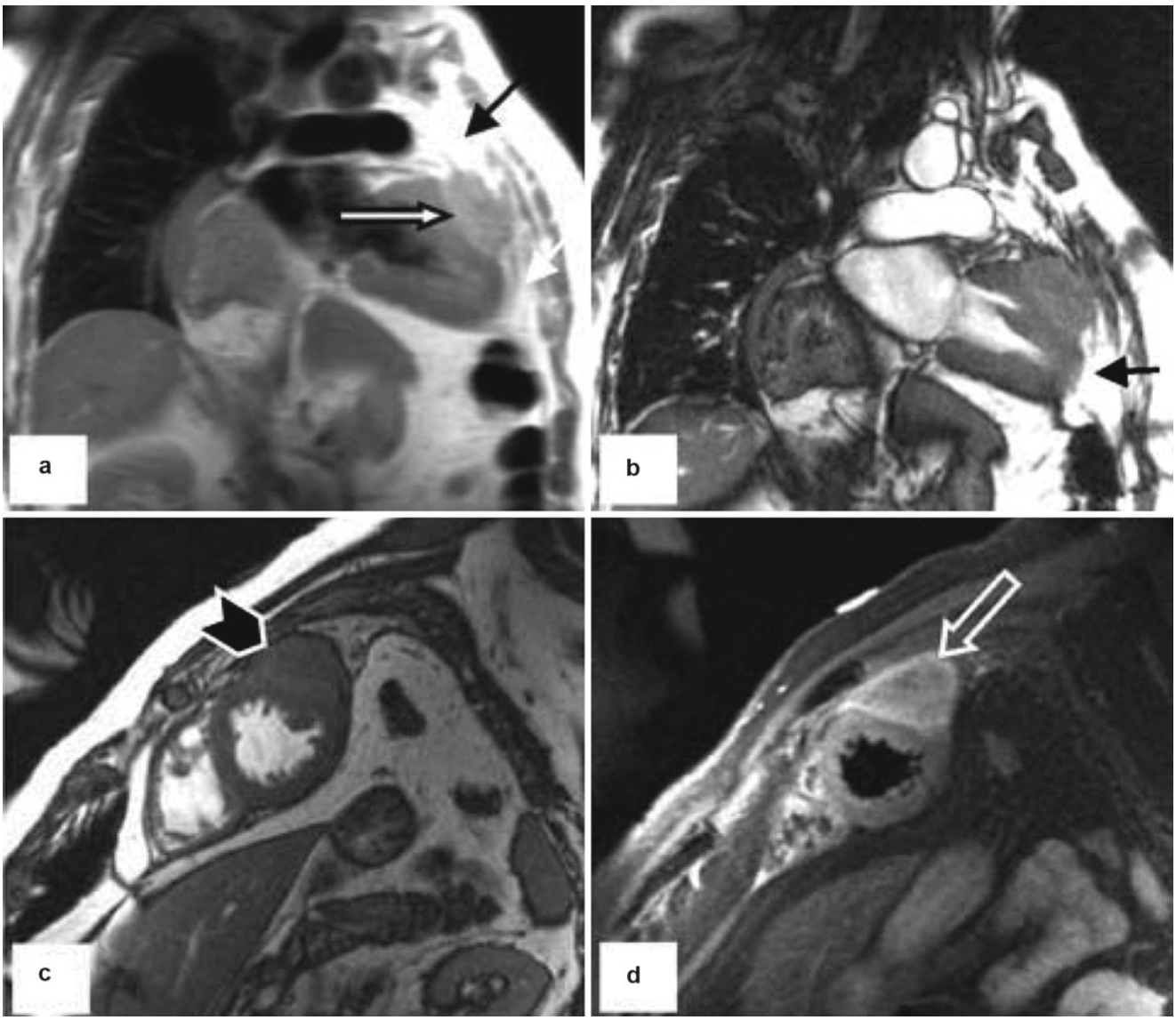

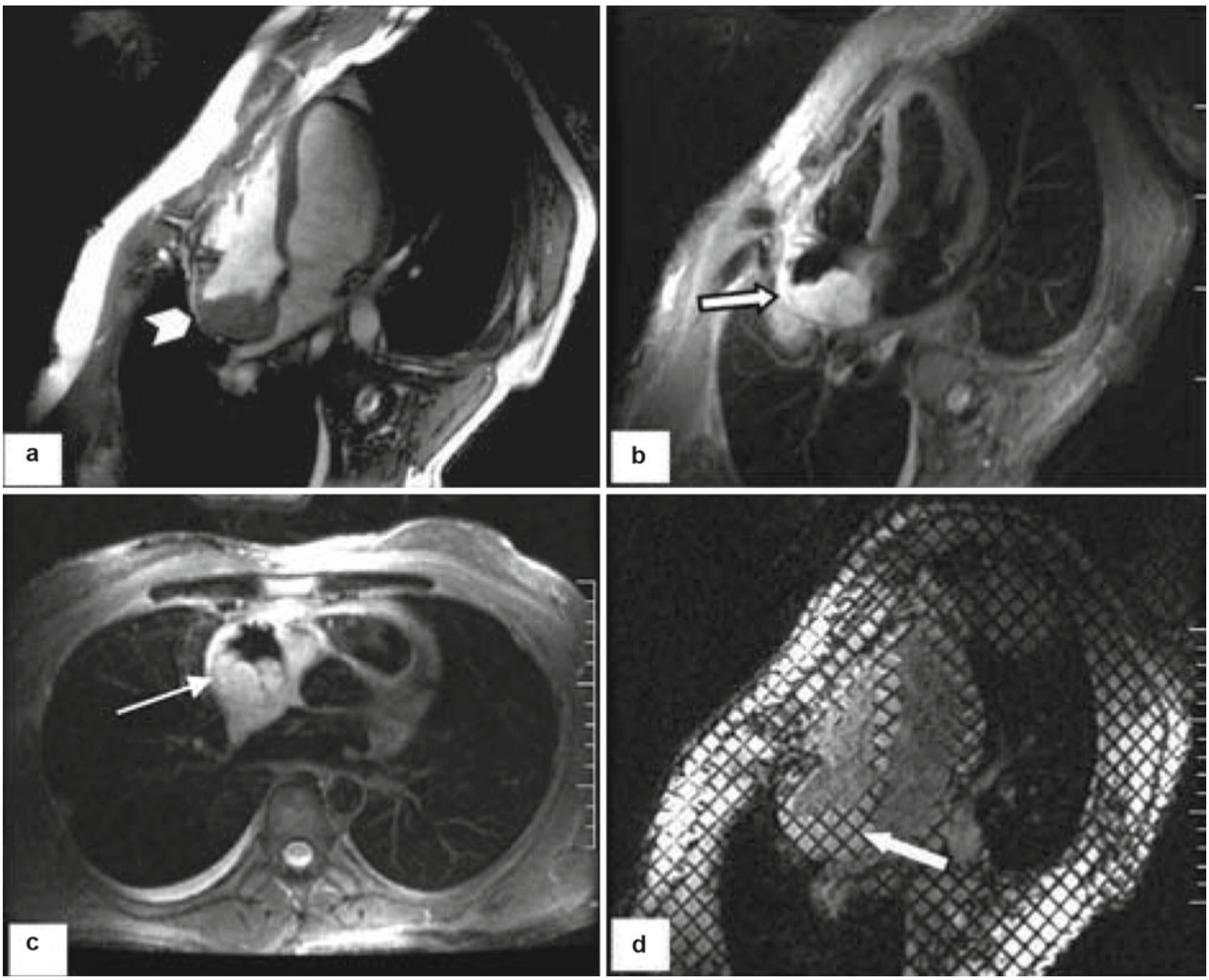

Fig. 13.21 A 39-year-old with chronic cough and fullness in the upper airway for several months presented after a CT scan revealed a mediastinal mass. Mediastinoscopy/biopsy revealed a small-cell carcinoma, but the proximity to the cardiac structures was unclear. The CMR data show that the mediastinal mass has invaded through the pericardium and deep into the right atrium (*arrows*). (**a**) Demonstrates SSFP (**b**) and (**c**) T2 weighting shows the extracardiac mass and (**c**) shows the multilobed nature of the invading mass. (**d**) RF tissue tagging demonstrates the mechanical properties of the mass and the interrelationship to the myocardium

Future Applications

We are far from exhausting the potential of MR and CT methods in applications to the cardiovascular system. As noted, it is now possible to obtain reasonable-quality images of the proximal coronary arteries. There is substantial work in progress to generate myocardial perfusion images using a bolus injection of gadolinium chelate at rest and with vasodilator stress using dipyridamole, adenosine, or regadenoson. This has provided accuracies similar to those obtained with

Fig. 13.20 A 73-year-old male who presented with several months of progressive chest discomfort was eventually diagnosed with small-cell carcinoma and underwent resection. He returned 8 month later for follow-up. A CT scan demonstrated a mass adjacent to the heart but was unable to distinguish invasion. (**a**) Demonstrates the large anterior oval mass (*large arrow*). The pericardium is clearly breached (*small arrows* **a–b**). (**c**) SSFP imaging demonstrated a loss of epicardial/mass continuity with penetration through the pericardium observed (*chevron*). (**d**) Late enhancement of the lesion (*arrow*) and the LV epicardial effacement. The CMR images demonstrated pericardial breaching and loss of epicardial border, and other images (not shown) depicted clear epicardial invasion, including tagged images portraying dyssynchronous motion of the tumor with impairment of the epicardial fibers, confirming lack of a separating surgical plane. The patient was deemed not a surgical candidate due to invasion, the high complexity, and risk of surgical resection

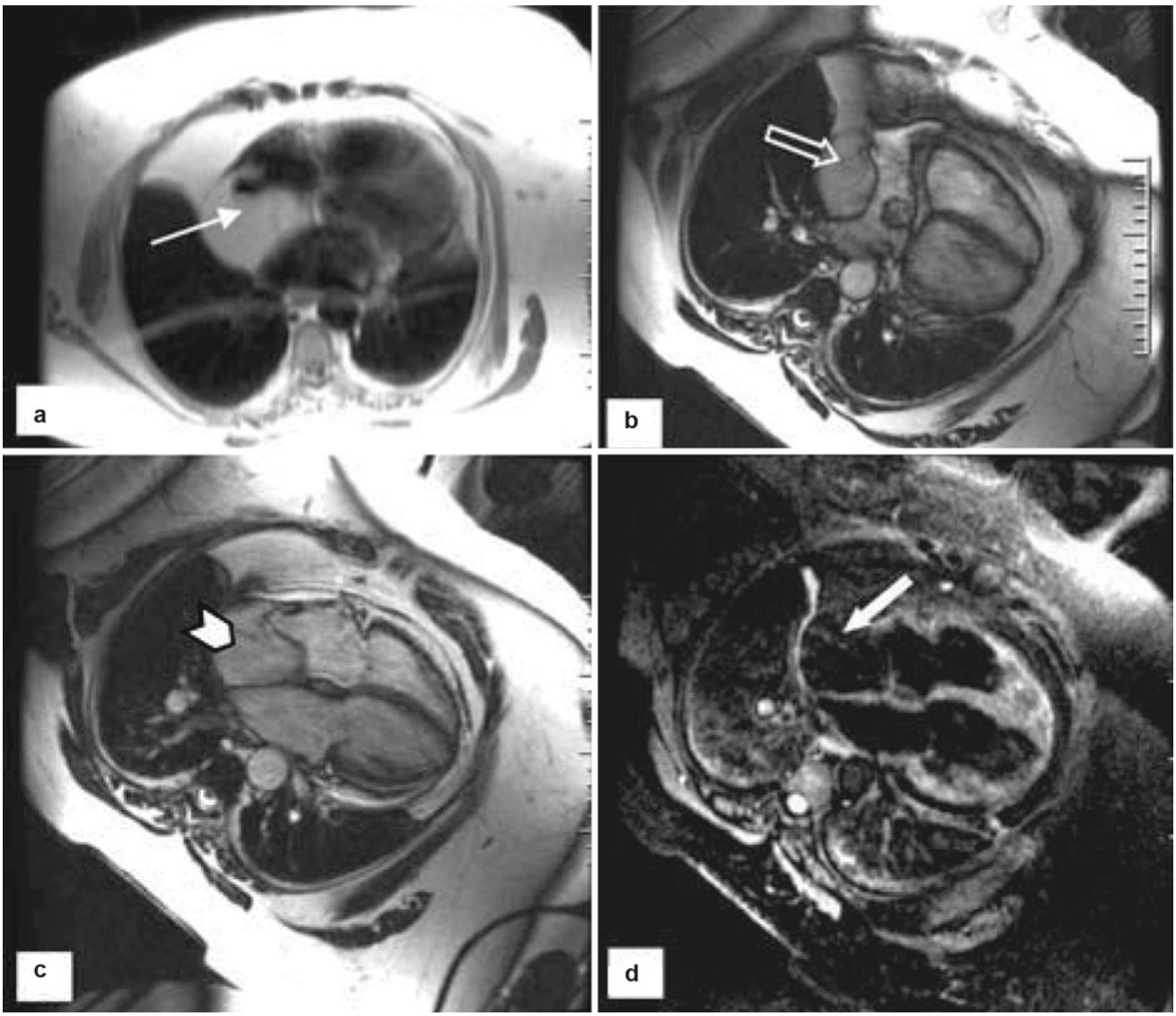

Fig. 13.22 A 65-year-old female presented with shortness of breath and mild SVC syndrome and was shown to have a mass on CT involving the right atrium and confirmed by TEE. For further evaluation, the patient underwent CVMRI. (**a** and **b**) demonstrate a large homogeneous mass occupying a large segment of the RA as well as considerable anterior mediastinal extrapericardial tissue, all bright on spin-echo imaging (proton density weighted). (**c**) An SSFP sequence demonstrated the obliteration of the posterior RA. Not shown is the near obliteration of the SVC. (**d**) The benign pathology of this presentation in this obese patient is confirmed by the T2-weighted image demonstrating uniform nulling of the tissue, which is diagnostic of a large fatty lipoma. Note the capsule surrounding the mass, which is a characteristic feature, differentiating it from lipomatous inner atrial hypertrophy. Diet and weight loss with exercise were recommended as an interim solution to forestall surgical resection for this otherwise benign lipoma with nonneoplastic but "malignant" features

the radiopharmaceuticals ^{201}Tl thallous chloride and ^{99m}Tc sestamibi or similar technetium-labeled compounds. CMR gadolinium perfusion may also have a role in identifying myocarditis (Fig. 13.27) or pericarditis and is the reference standard now for myocardial viability. MRS is another unique diagnostic modality that can assess myocardial metabolism without the need for ionizing radiation or administration of intravenous tracer or contrast agents. The ultimate potential for clinical application of ^{31}P MRS is the detection of myocardial ischemia using the evaluating the transient imbalance between oxygen supply and demand by measuring high-energy phosphate. Noninvasive MRS has been suggested to be complimentary to myocardial biopsy and has characterized various myocardial pathologies such as cardiac rejection, in vivo differentiation between cardiac rejection and acute myocardial ischemia, evaluation of dilated/hypertrophic cardiomyopathy or valvular disease, and various microvascular diseases [16, 37]. As MR paramagnetic contrast techniques evolve and MR "tracer" approaches using nanotechnology and other approaches

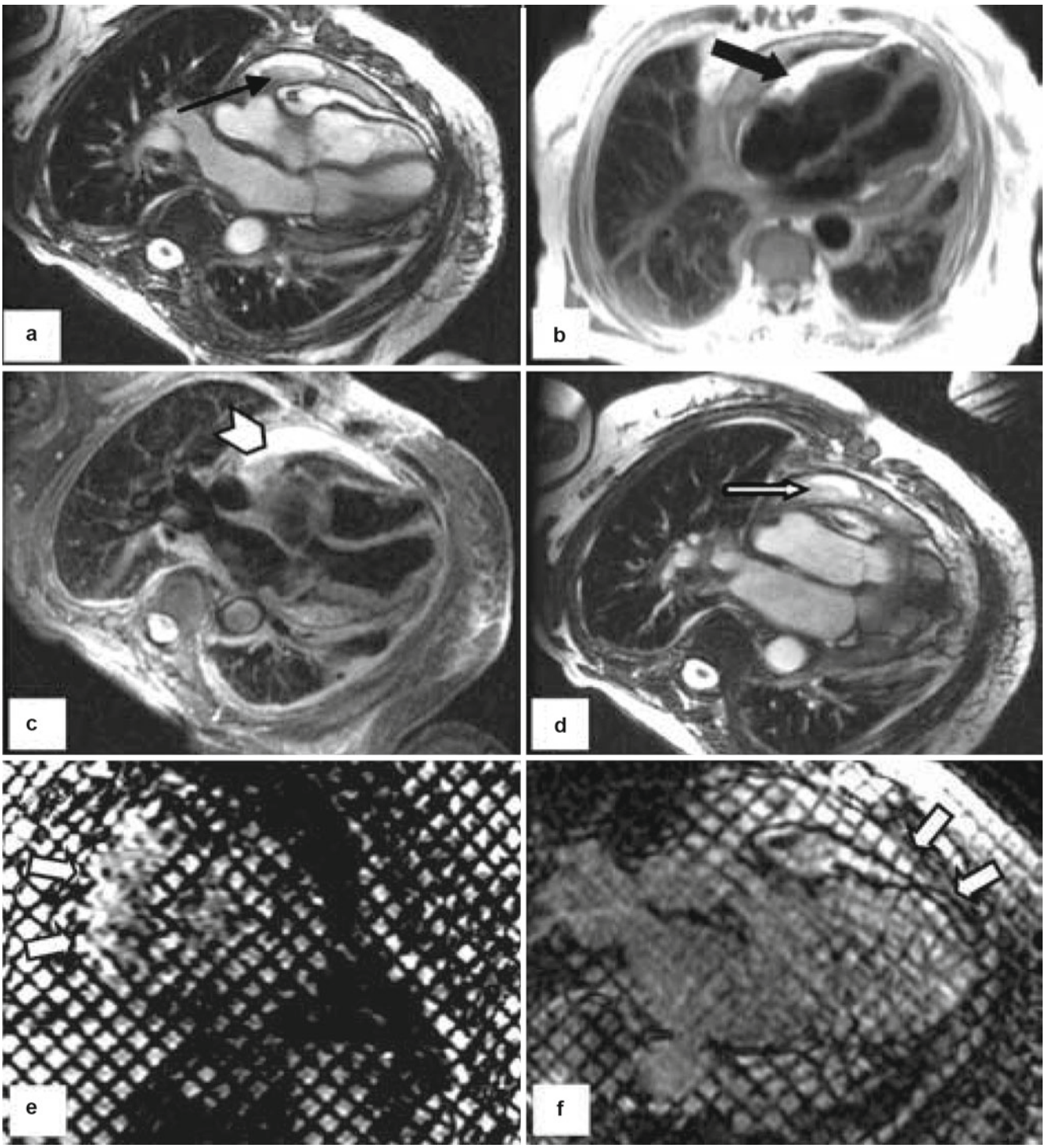

Fig. 13.23 This patient had a restrictive cardiomyopathy. (**a**) Demonstrates a pericardial effusion (*arrow*), which, when combined with (**b–d**), is better described as an effusive-constrictive pericarditis, as evidenced by fibrinous stranding and the densely adherent fibrous nature intermixed with the effusion (*arrows*, **b–d**). Radio frequency tissue tagging (*arrows*, **e**, **f**) demonstrates the adherence between the visceral and parietal pericardia, as evidenced by the absence of slippage and deformation of the *tag lines*, confirming the finding of a constrictive anatomy and physiology that was confirmed at surgery

develop and as the use of systems using higher magnetic fields progress, the opportunity for further creative applications of CMR will expand. Furthermore, CT applications have improved substantially, since the development of 64-slice MDCT and more advanced CT systems with up to 320-slice capability. Further development of CT stress perfusion and fractional flow reserve methods (FFR-CT) will take CT from its present status of anatomic imaging to the

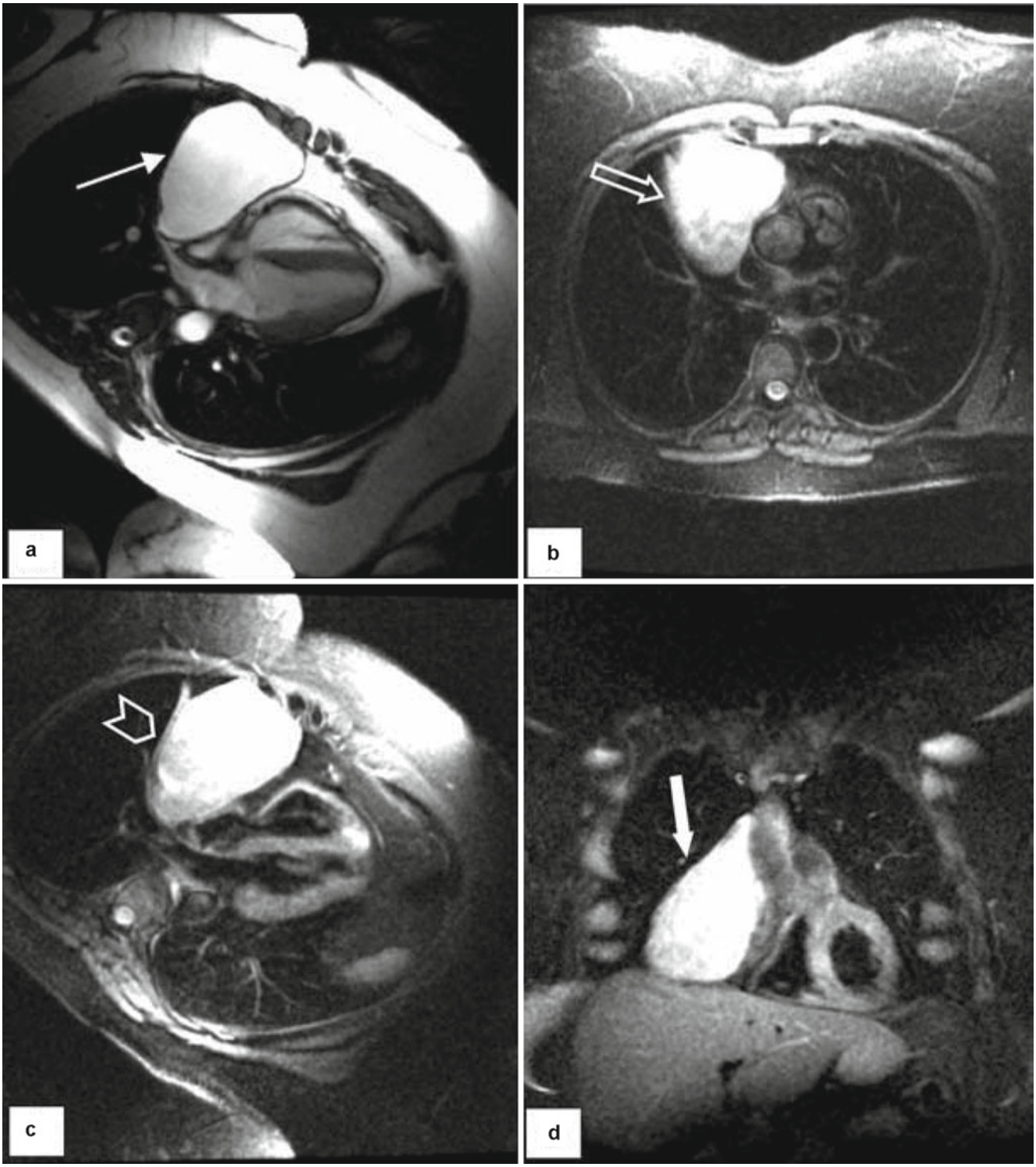

Fig. 13.24 A 45-year-old female was followed for several years by CT and TEE for this right-sided homogeneous, well-circumscribed, and encapsulated mass (*arrows*, **a**–**d**). (**a**) The bright signal characteristic on T1 imaging is seen and in (**b**) the lack of nulling on T2 imaging, consistent with its cystic nature (**c** and **d**). In (**c** and **d**) note the proper nulling of epicardial fat adjacent to mass (*chevron*). Tissue characteristics, as well as the anatomic position, make this mass pathognomonic for a pericardial cyst, which is large but benign

additional ability to add physiologic information. As such, CT could provide information complementary to that of CMR. Nonetheless, the advantage of CMR as a methodology that, like ultrasound, has no ionizing radiation gives CMR a remarkable advantage as an overall imaging modality. Ultimately, appropriate use and new applications of these remarkable two advanced imaging technologies will solidify their place in the armamentarium of the clinician.

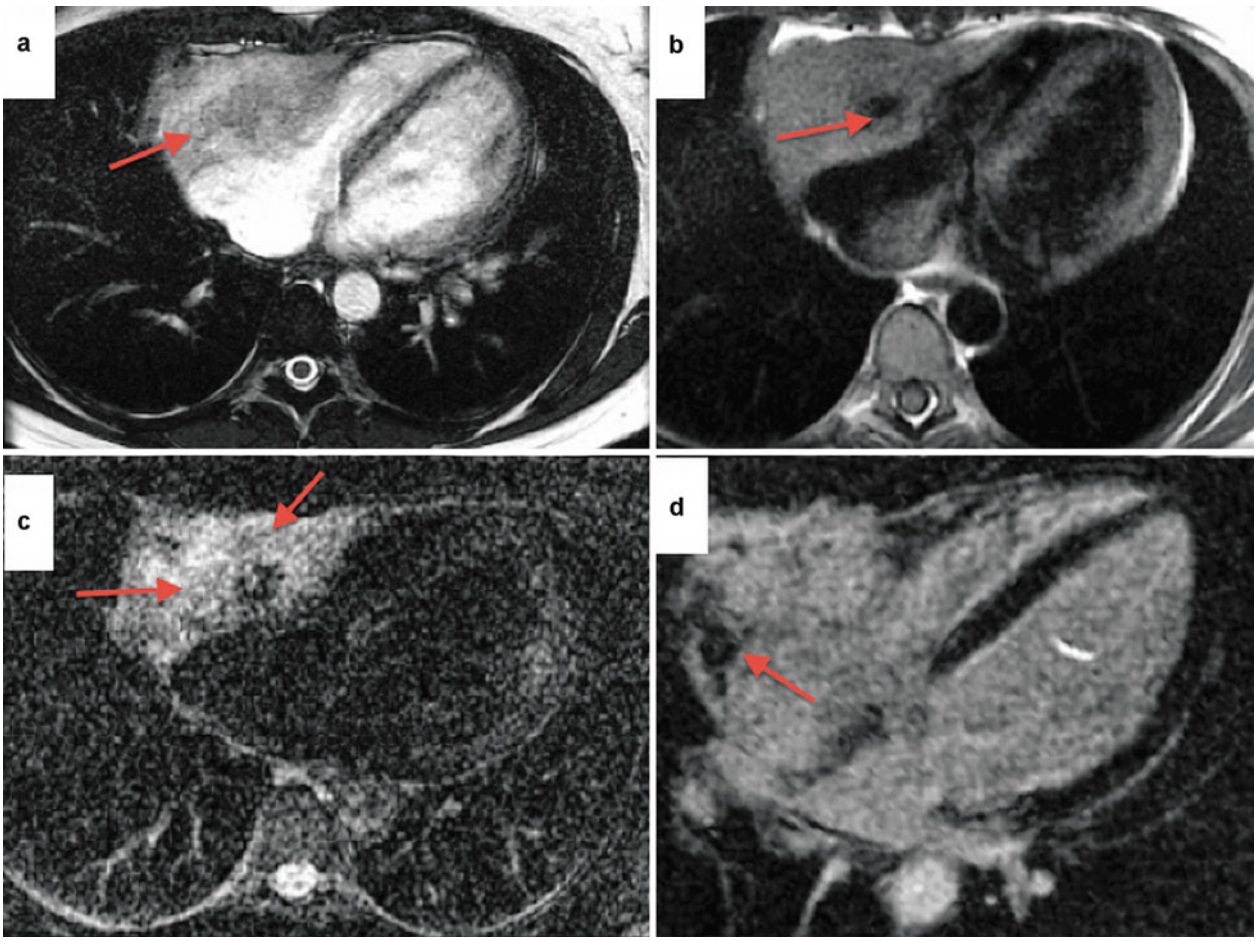

Fig. 13.25 A 40-year-old female with atypical chest pain and non-sustained ventricular tachycardia underwent CMR for evaluation of a right atrioventricular groove mass. (**a**) Axial SSFP cine showing a large heterogeneous mass invading the right atrium and ventricle (*arrow*). (**b**) Axial T1-weighted DIR fast spin echo depicting a void (*arrow*) within the mass thought to be the encased and dilated right coronary artery. (**c**) Axial T2-weighted image showing high water signal within the mass consistent with a highly vascular malignancy (*arrow*). (**d**) Four-chamber delayed enhancement showing area of nulling within the mass thought to be necrotic material or thrombus (*arrow*). The tumor was biopsied and histology revealed a primary cardiac angiosarcoma

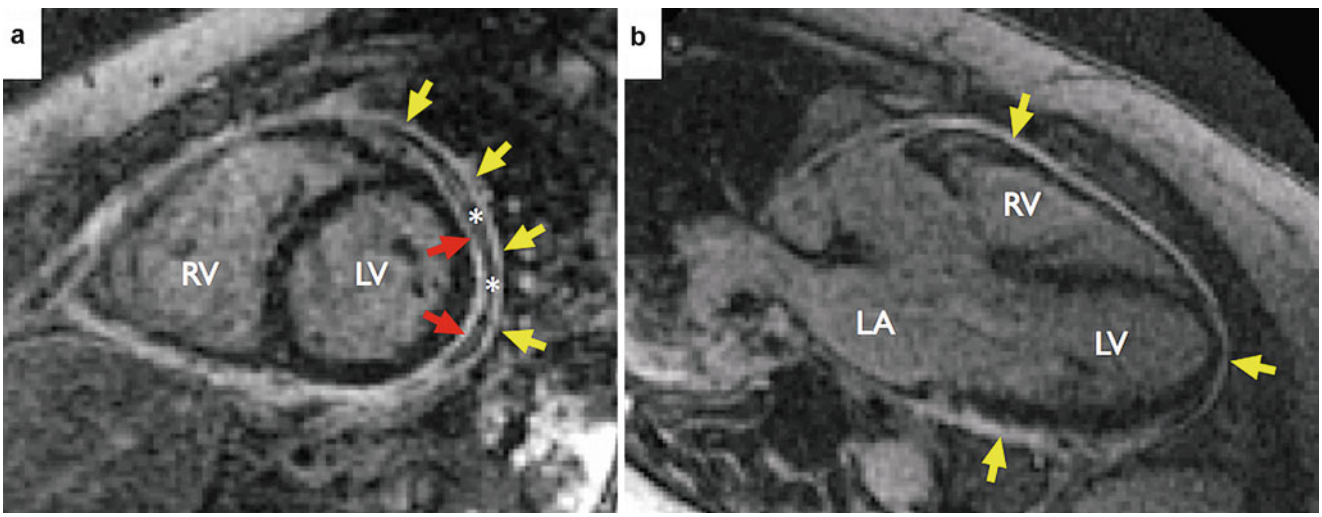

Fig. 13.26 Delayed enhancement images in mid-level short-axis (**a**), three-chamber (**b**), two-chamber (**c**), and four-chamber (**d**) orientations. These images demonstrate delayed enhancement of the parietal pericardium (*yellow arrows*), visceral pericardium (*red arrows*), and a small pericardial effusion (*asterisks*) consistent with acute pericarditis

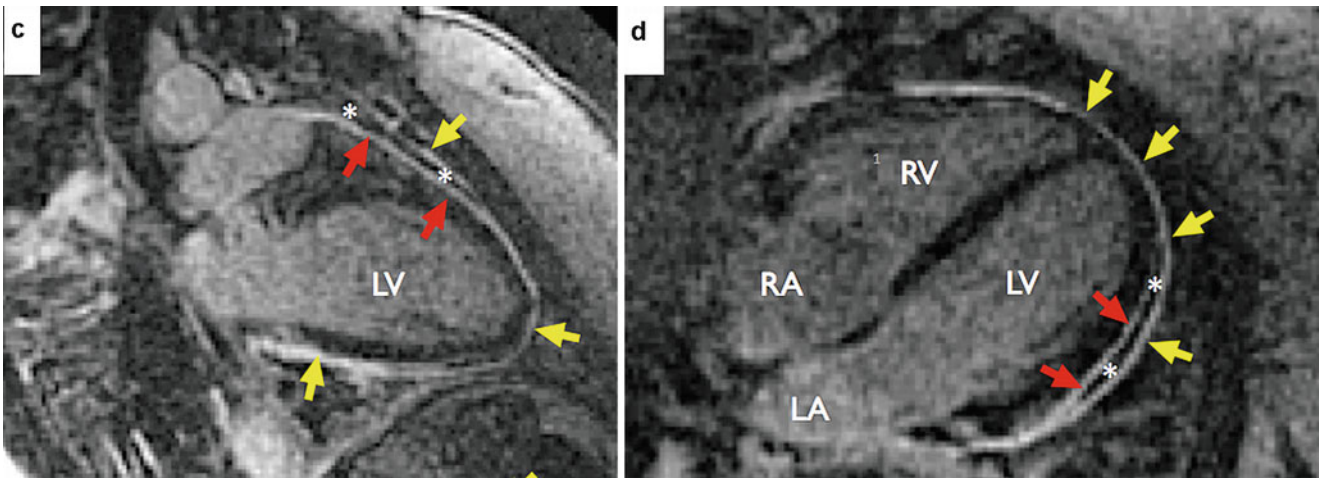

Fig. 13.26 (continued)

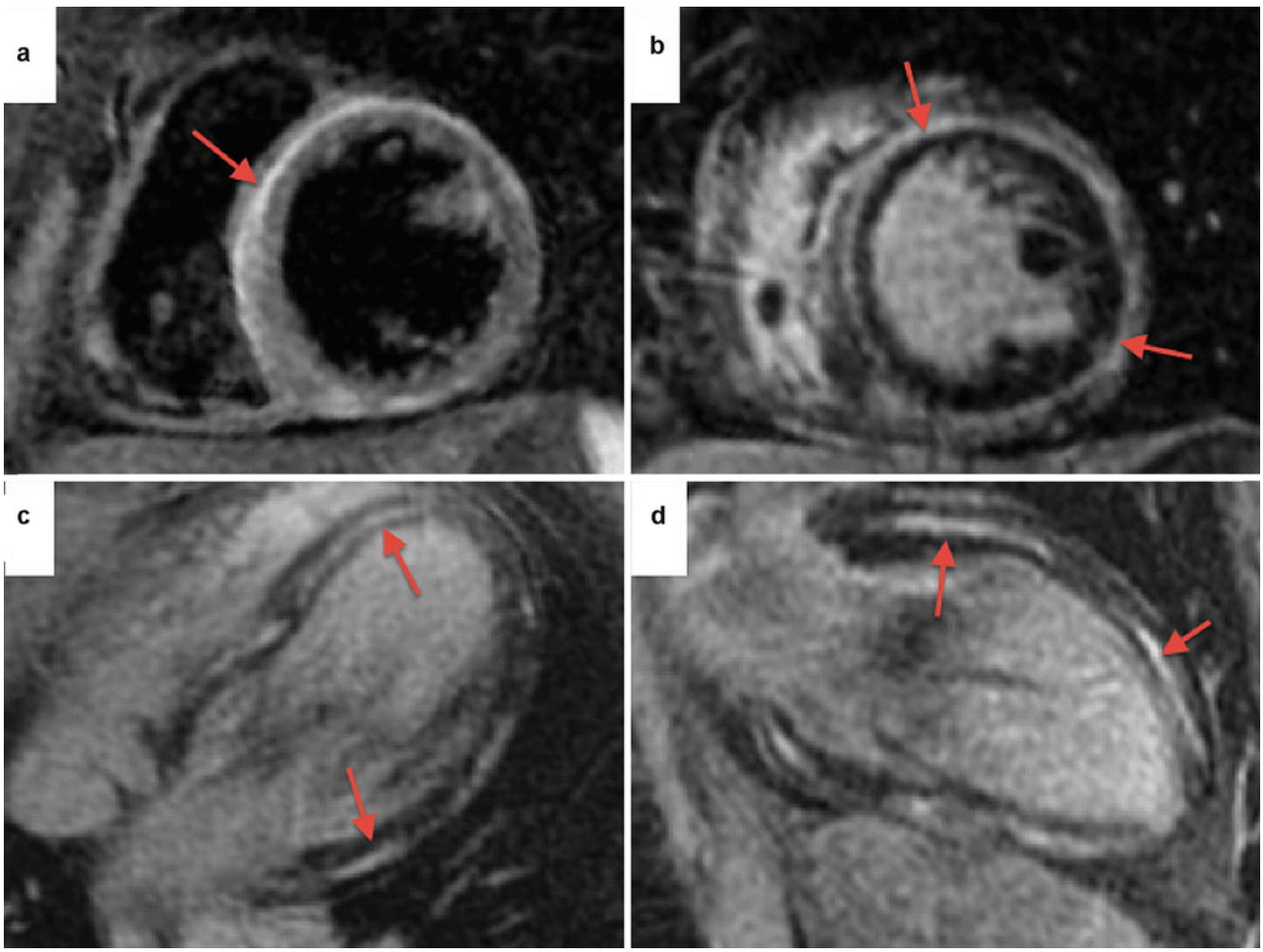

Fig. 13.27 An 18-year-old female was admitted with severe chest pain and elevated serum troponin and normal coronary arteries by angiography. (**a**) Short-axis T2-weighted inversion recovery sequence showing near-circumferential signal increase consistent with myocardial edema (*red arrows*, **a**–**d**). (**b**) Short-axis delayed enhancement sequence at a similar ventricular level to (**a**) showing circumferential mid-wall enhancement typical for acute myocarditis. Four-chamber (**c**) and two-chamber (**d**) delayed enhancement sequence showing patchy areas of mid-wall and epicardial enhancement

Conclusions

Cardiac MR and CT (Table 13.1) have been available for clinical use since the early 1980s. Advances in both have been achieved throughout the years. CMR has proven to be the more versatile, owing to its ability to use a number of contrast mechanisms, whereas CT methods rely only on X-ray attenuation. Both technologies have substantial clinical utility, however, and can often be used for similar diagnostic applications. When a facility has only CMR or CT, it may be possible to use that modality as the primary diagnostic study. If the advances of the past decade are any indication, both techniques are poised for substantial breakthroughs in cardiovascular imaging for improving speed, resolution, and diagnostic accuracy.

References

1. Pohost GM, O'Rourke RA, editors. Basic principles of magnetic resonance. Principles and practice of cardiovascular imaging. Boston: Little, Brown; 1990.
2. Cranney GB, Lotan CS, Dean L, et al. Left ventricular volume measurements using cardiac axis nuclear magnetic imaging: validation by calibrated ventricular angiography. Circulation. 1990;52:154–63.
3. Dell'Italia LI, Blackwell GC, Pearce WI, Pohost GM. Assessment of ventricular volumes using cine magnetic resonance in the intact dog. A comparison of measurement methods. Invest Radiol. 1994;2:162–6.
4. Benjelloun H, Cranney GB, Kirk KA, et al. Interstudy reproducibility of biplane cine nuclear magnetic resonance measurements of left ventricular function. Am J Cardiol. 1991;67:1413–9.
5. Nagel E, Schneider U, Schalla S, et al. Magnetic resonance real-time imaging for the evaluation of left ventricular function. J Cardiovasc Magn Reson. 2000;2:7–14.
6. Bottini PB, Can AA, Prisant LM, et al. Magnetic resonance imaging compared to echocardiography to assess left ventricular mass in the hypertensive patient. Am J Hypertens. 1995;8:221–8.
7. Young AA, Kramer CM, Ferrari VA, et al. Three-dimensional left ventricular deformation in hypertrophic cardiomyopathy. Circulation. 1994;90:854–67.
8. Marcus JT, Gotte LW, DeWaal LK, et al. The influence of through-plane motion on left ventricular volumes measured by magnetic resonance imaging: implications for image acquisition and analysis. J Cardiovasc Magn Reson. 1999;1:1–6.
9. Schroeder S, Kopp AF, Kuettner A, et al. Influence of heart rate on vessel visibility in noninvasive coronary angiography using new multislice computed tomography: experience in 94 patients. Clin Imaging. 2002;26:106–11.
10. Fayad ZA, Fuster V, Nikolaou K, Becker C. Computed tomography and magnetic resonance imaging for noninvasive coronary angiography and plaque imaging: current and potential future concepts. Circulation. 2002;106:2026–34.
11. Morin RL, Gerber TC, McCollough CH. Radiation dose in computed tomography of the heart. Circulation. 2003;107:917–22.
12. Becker CR, Knez A, Ohnesorge B, et al. Imaging of noncalcified coronary plaques using helical CT with retrospective ECG gating. AJR Am J Roentgenol. 2000;175:423–4.
13. Fujita N, Duerinckx AJ, Higgins CB. Variation in left ventricular wall stress with cine magnetic resonance imaging: normal subjects versus dilated cardiomyopathy. Am Heart J. 1993;125(5 Pt 1):1337–44.
14. Wu E, Judd RM, Vargas JD, et al. Visualisation of presence, location, and transmural extent of healed Q-wave and non-Q-wave myocardial infarction. Lancet. 2001;357:21–8.
15. Kim RJ, Wu E, Rafael A, et al. The use of contrast-enhanced magnetic resonance imaging to identify reversible myocardial dysfunction. N Engl J Med. 2000;343:1445–53.
16. Wang Y, Qin L, Shi X, Zeng Y, Jing H, Schoepf UJ, et al. Adenosine-stress dynamic myocardial perfusion imaging with second-generation dual-source CT: comparison with conventional catheter coronary angiography and SPECT nuclear myocardial perfusion imaging. AJR Am J Roentgenol. 2012;198(3):521–9.
17. van Rugge FP, van der Wall EE, Spanjersberg SJ, et al. Magnetic resonance imaging during dobutamine stress for detection and localization of coronary artery disease. Quantitative wall motion analysis using a modification of the centerline method. Circulation. 1994;90:127–38.
18. Chiu CW, So NMC, Lam WWM, et al. Combined first-pass perfusion and viability study at MR imaging in patients with non-ST segment- elevation acute coronary syndromes: feasibility study. Radiology. 2003;226:717–22.
19. Baer FM, Voth E, Theissen P, et al. Gradient-echo magnetic resonance imaging during incremental dobutamine infusion for the localization of coronary artery stenoses. Eur Heart J. 1994;15:218–25.
20. Wilke N, Jerosch-Herold M, Stillman AE, et al. Concepts of myocardial perfusion imaging in magnetic resonance imaging. Magn Reson Q. 1994;10:249–86.
21. Schmermund A, Beli MR, Lerman LO, et al. Quantitative evaluation of regional myocardial perfusion using fast x-ray computed tomography. Herz. 1997;22:29–39.
22. Bastarrika G, Ramos-Duran L, Rosenblum MA, Kang DK, Rowe GW, Schoepf UJ. Adenosine-stress dynamic myocardial CT perfusion imaging: initial clinical experience. Invest Radiol. 2010;45(6):306–13.
23. Blankstein R, Shturman LD, Rogers IS, Rocha-Filho JA, Okada DR, Sarwar A, et al. Adenosine-induced stress myocardial perfusion imaging using dual-source cardiac computed tomography. J Am Coll Cardiol. 2009;54(12):1072–84.
24. Vorobiof G, Achenbach S, Narula J. Minimizing radiation dose for coronary CT angiography. Cardiol Clin. 2012;30(1):9–17.
25. Kopp AF, Schroeder S, Kuettner A, et al. Non-invasive coronary angiography with high resolution multi-detector-row computed tomography. Eur Heart J. 2002;23:1714–25.
26. Schmermund A, Bailey KR, Rumberger JA, et al. An algorithm for noninvasive identification of angiographic three-vessel and/or left main coronary artery disease in symptomatic patients on the basis of cardiac risk and electron-beam computed tomographic calcium scores. J Am Coll Cardiol. 1999;33:444–52.
27. Callister TQ, Raggi P, Cooil B, et al. Effect of HMG-CoA reductase inhibitors on coronary artery disease as assessed by electron-beam computed tomography. N Engl J Med. 1998;339:1972–8.
28. Woo P, Mao S, Wang S, Detrano RC. Left ventricular size determined by electron beam computed tomography predicts significant coronary artery disease and events. Am J Cardiol. 1997;79:1236–8.
29. Rumberger JA, Brundage BH, Rader DJ, Kondos G. Electron beam computed tomographic coronary calcium scanning: a review and guidelines for use in asymptomatic persons. Mayo Clin Proc. 1999;74:243–52.
30. O'Rourke RA, Brungate BH, Froelicher VF, et al. American College of Cardiology/American Heart Association expert consensus document on electron-beam computed tomography for the

diagnosis and prognosis of coronary artery disease. J Am Coll Cardiol. 2000;36:326–40.
31. Detrano RC, Wong ND, Doherty TM, et al. Coronary calcium does not accurately predict near-term future coronary events in high-risk adults. Circulation. 1999;99:2633–8.
32. Budoff MI, Shavelle DM, Lamont DH, et al. Usefulness of electron beam computed tomography scanning for distinguishing ischemic from nonischemic cardiomyopathy. J Am Coll Cardiol. 1998;32: 1173–8.
33. Yamaguchi H, Nishiyama S, Nakanishi S, Nishimura S. Electrocardiographic, echocardiographic and ventriculographic characterization of hypertrophic non-obstructive cardiomyopathy. Eur Heart J. 1983;4(Suppl F):105–19.
34. Grobner T. Gadolinium – a specific trigger for the development of nephrogenic fibrosing dermopathy and nephrogenic systemic fibrosis? Nephrol Dial Transplant. 2006;21:1104–8.
35. Fujita N, Chazoulliers AE, Hartialia JJ. Quantification of mitral regurgitation by velocity encoding cine nuclear magnetic resonance imaging. J Am Coll Cardiol. 1994;23:951–2.
36. Friedrich MG, Strohm O, Schuiz-Menger I, et al. Contrast media-enhanced magnetic resonance imaging visualizes myocardial changes in the course of viral myocarditis. Circulation. 1998;97: 1802–9.
37. Beer M, Seyfarth T, Sandstede J, et al. Absolute concentrations of high-energy phosphate metabolites in normal, hypertrophied, and failing human myocardium measured noninvasively with 31P-SLOOP magnetic resonance spectroscopy. J Am Coll Cardiol. 2002;40:1267–74.

Recommended Reading

Detrano RC, Wong ND, Doherty TM, et al. Coronary calcium does not accurately predict near-term future coronary events in high-risk adults. Circulation. 1999;99(20):2633–8.
Forder JR, Pohost GM. Cardiovascular nuclear magnetic resonance: basic and clinical applications. J Clin Invest. 2003;111:1630–9.
Kim HW, Lee D, Pohost GM. 31P cardiovascular magnetic resonance spectroscopy: a unique approach to the assessment of the myocardium. Future Cardiol. 2009;5:523–7.
Manning WJ, Pennell DJ. Cardiovascular magnetic resonance. New York: Churchill Livingstone; 2002.
Manning WJ, Li W, Edelman RR. A preliminary report comparing magnetic resonance coronary angiography with conventional angiography. N Engl J Med. 1993;328:828–32.
Martin ET, Fuisz AR, Pohost GM. Imaging cardiac structure and pump function. Cardiol Clin. 1998;16:135–60.
Ohnesorge BM, Becker CR, Flohr TG, Reiser MF. Multislice CT cardiac imaging. Berlin: Springer; 2002.
O'Rourke RA, Brundage BH, Froelicher VF, et al. American College of Cardiology/American Heart Association Expert Consensus document on electron-beam computed tomography for the diagnosis and prognosis of coronary artery disease. J Am Coll Cardiol. 2000;36:326–40.
Pohost GM, Hung L, Doyle M. Clinical use of cardiovascular magnetic resonance; special review, clinician update. Circulation. 2003;108: 647–53.